1 H), 3.72 (d, J = 7 Hz, 1 H), 3.76 (s, 3 H), 3.88 (d, J = 7 Hz, 1 H), 4.58 (s, 1 H); IR (thin film) 2985, 2882, 1783, 1767, 1466, 1437, 1393, 1366, 1200, 1100 cm^{-1}; mass spectrum (CI$^+$, isobutane) m/z (relative intensity) 188 (M + 1, 50), 128 (100), 116 (20), 74 (10). Anal. Calcd for $C_9H_{17}NO_3$: C, 57.74; H, 9.15; N, 7.48. Found: C, 57.49; H, 9.18; N, 7.33. A 0.5 M solution of **3** in benzene had an optical density at 337 nm of less than 0.02.

3-Ethyl-2,4,4-trimethyl-1,3-oxazolidine (4). 2-(Ethylamino)-2-methylpropanol was prepared as described by Benson and co-workers.[7] Acetaldehyde (13.83 g, 0.314 mol) was added to a round-bottom flask containing 9.20 g (0.0786 mol) of 2-(ethylamino)-2-methylpropanol in 200 mL of benzene at ambient temperature. The flask was equipped with a Dean-Stark head, and the reaction mixture was heated at reflux with stirring until no additional water was collected. Pure **4** was obtained as a colorless liquid (9.33 g, 83%) by vacuum distillation at 55 °C at 8 Torr. The product was characterized from the following data: ^{1}H NMR ($CDCl_3$) δ 0.98 (s, 3 H), 1.04 (t, X of ABX_3 pattern, $J_{AX} = J_{BX}$ = 7 Hz, 3 H), 1.09 (s, 3 H), 1.23 (d, J = 5 Hz, 3 H), 2.28 (A of ABX_3, J_{AB} = 13, J_{AX} = 7 Hz, 1 H), 2.59 (B of ABX_3, J_{AB} = 13 Hz, J_{BX} = 7 Hz, 1 H), 3.52 (d, J = 7 Hz, 1 H), 3.58 (d, J = 7 Hz, 1 H), 4.26 (q, J = 5 Hz, 2 H); IR (thin film) 2974, 2594, 1464, 1393, 1302, 1026, 976, 934, 862, 834, 740, 649 cm^{-1}; mass spectrum (EI$^+$) m/z (relative intensity) 143 (3), 142 (4), 129 (5), 128 (49), 114 (12), 100 (19), 86 (100), 84 (20), 74 (14), 58 (42), 42 (27); high resolution M$^+$, m/z 143.1299; calcd for $C_8H_{17}NO$, m/z 143.1310. A 0.5 M solution of the purified **4** had an optical density at 337 nm of less than 0.02.

Bi(2-carbomethoxy-3-ethyl-4,4-dimethyl-1,3-oxazolidin-2-yl). A 20 mm o.d. × 200 mm quartz tube was charged with 2.1 g (11 mmol) of 3-ethyl-4,4-dimethyl-2-carbomethoxyoxazolidine (**3**), 0.82 g (5.6 mmol) of di-*tert*-butyl peroxide, and 65 mL of spectral grade benzene and equipped with a reflux condenser. The solution was oxygen degassed with prepurified argon for 10 min and irradiated with continuous degassing for 24 h in a Rayonet Photochemical Reactor (Model RPR 100, Southern New England Ultraviolet Co., Hamden, CT) equipped with sixteen 3000-Å lamps. The solvent was removed by rotary evaporation and the residue was purified by flash chromatography with use of a 30 mm o.d. flash column eluting with 20% ethyl acetate/hexanes (v/v). The desired fractions were combined and the solvent rotary evaporated. After air drying 0.60 g (29%) of bi(2-carbomethoxy-3-ethyl-4,4-dimethyl-1,3-oxazolidin-2-yl) was collected as a mixture of meso and *dl* isomers. The ^{1}H NMR spectrum in $CDCl_3$ showed both stereoisomers: (major isomer, 75%) δ 1.16 (t, X of ABX_3 pattern, $J_{AX} = J_{BX}$ = 7 Hz, 6 H), 1.28 (s, 6 H), 1.35 (s, 6 H), 2.64 (A of ABX_3, J_{AB} = 12 Hz, J_{BX} = 7 Hz, 2 H), 3.12 (B of ABX_3, J_{AB} = 12 Hz, J_{BX} = 7 Hz, 2 H), 3.72 (d, J = J Hz, 1 H), 3.70 (s, 6 H), 3.94 (d, J = 7 Hz, 2 H), 4.14 (s, 2 H); (minor isomer, 25%) δ 1.05 (t, X of ABX_3, $J_{AX} = J_{BX}$ = 7 Hz, 6 H), 3.70, (s, 6 H), the other peaks overlapped with the major isomer; mass spectrum (CI$^+$, isobutane) m/z (relative intensity) 285 (M + 1, 35), 185 (10), 142 (100). Anal. Calcd for $C_{18}H_{32}N_2O_6$: C, 58.05; H, 8.66; N, 7.52. Found: C, 57.92; H, 8.70; N, 7.53.

Attempts To Form 2-Carbomethoxy-3-ethyl-4,4-dimethyl-1,3-oxazolidin-2-yl from Bi(2-carbomethoxy-3-ethyl-4,4-dimethyl-1,3-oxazolidin-2-yl). Bi(2-carbomethoxy-3-ethyl-4,4-dimethyl-1,3-oxazolidin-2-yl) (5 mg) was dissolved in 2 mL of a 1 M solution of silver nitrate in methanol. No metallic silver was formed even upon heating a solution to 100 °C. No EPR signal was observed upon heating an ethanol solution of bi(2-carbomethoxy-3-ethyl-4,4-dimethyl-1,3-oxazolidin-2-yl) to 70 °C in the cavity of an EPR spectrometer.

Photoacoustic Calorimetry. The photoacoustic apparatus has been described in detail elsewhere.[20-22] Solutions were photolyzed by a Molectron UV24 pulsed nitrogen laser (337.1 nm, 10 ns pulse width) and the resulting shock waves were detected by a Panametrics V101 transducer (2 μs response), amplified by a Panametrics Model 5670 ultrasonic preamplifier and signal averaged with a Tektronix Model 7D20 digital oscilloscope. Optical densities were measured with a Hewlett-Packard Model 8450 diode array spectrometer. In all cases, the slope from a plot of the normalized photoacoustic signal versus $(1-10^{-OD})$, where OD is the optical density of the solution at 337 nm, was linear with a correlation coefficient >0.999. The observed fraction of heat deposited in solution, α_{obs}, was the ratio of the slope of this line for reaction 3 versus that for *o*-hydroxybenzophenone.

Acknowledgment. We gratefully acknowledge Dr. Linda J. Johnston for the use of the laser flash photolysis apparatus. S.H.D. and T.H.K. thank the U.S. National Science Foundation (Grant No. 9201075) for financial support. We thank Dr. Olester Benson, Jr., for preparing the sample of **3** for combustion analysis.

The Temperature and Medium Dependencies of *cis*-Stilbene Fluorescence. The Energetics for Twisting in the Lowest Excited Singlet State

Jack Saltiel,* Andrew S. Waller, and Donald F. Sears, Jr.

Contribution from the Department of Chemistry, The Florida State University, Tallahassee, Florida 32306-3006. *Received September 18, 1992*

Abstract: Fluorescence quantum yields of *cis*-stilbene-d_0 and -d_2 were measured as a function of temperature in *n*-hexane and *n*-tetradecane. *cis*-Stilbene fluorescence quantum yields were decomposed into emission contributions from ^{1}c*,ϕ_{fc}^c, and adiabatically formed ^{1}t*,ϕ_{ft}^c, by application of principal-component analysis. Rate constants, k_{cp} for the ^{1}c* → ^{1}p* torsional process, calculated from ϕ_{fc}^c give Arrhenius activation parameters E_{cp}^a = 0.33 ± 0.08 and 1.90 ± 0.08 kcal/mol and ln A = 27.80 ± 0.13 and 30.09 ± 0.12 for *n*-hexane (*c*-d_0 and *c*-d_2) and *n*-tetradecane (*c*-d_0), respectively. Deuteration of the olefinic positions has no effect on k_{cp} in *n*-hexane, but diminishes k_{cp} by ~10% in *n*-tetradecane. Applying the medium-enhanced barrier model on these k_{cp}'s and on literature k_{cp}'s in methylcyclohexane/methylcyclopentane gives $E_{cp}^a = -(1.07 \pm 0.05) + (0.89 \pm 0.01)E_{\eta_s}$ kcal/mol indicating a negative intrinsic barrier, $E_c^0 = -1.07 \pm 0.05$ kcal/mol, and a nearly full imposition of the activation energy for viscous flow, E_{η_s}, to the ^{1}c* → ^{1}p* process, independent of deuterium substitution at the olefinic positions. The ϕ_{ft}^c values are remarkably T independent in both solvents. Assuming that adiabatic formation of ^{1}t* takes the ^{1}c* → ^{1}p* → ^{1}t* pathway, these results indicate that ^{1}p* and ^{1}t* represent essentially isoenergetic regions in the potential energy surface of the lowest excited stilbene singlet state, thus providing the first experimental estimate of the energy of the perpendicular singlet state, ^{1}p*.

The effect of medium friction on the rates of very fast unimolecular reactions has been the topic of many recent experimental and theoretical investigations.[1] The trans ⇄ cis photoisomerization of stilbene is at the center of much of this work because

0002-7863/93/1515-2453$04.00/0

it affords the opportunity to determine the influence of the medium on barrier-controlled (trans side) and essentially barrierless (cis side) motions of potentially identical molecular moieties.[1] Isomerization of either stilbene isomer is assumed to proceed via torsional motion to intermediate $^1p^*$ whose equilibrium geometry corresponds to ~90° rotation about the central bond.[2] Anticipation of the elusive nature of this intermediate led to its being dubbed the phantom excited singlet state, an appropriate characterization given the many futile attempts to observe it. Torsional relaxation from the trans side, $^1t^* \rightarrow {}^1p^*$, has been studied most extensively and has been shown to be subject to an intrinsic barrier of ~3.0 kcal/mol both in the isolated molecule[3,4] and in hydrocarbon solvents.[5] Torsional relaxation from the cis side, $^1c^* \rightarrow {}^1p^*$, has been assumed to be essentially barrierless, based on previous failures to observe $^1c^*$ fluorescence and on the T independence of c → t and c → dihydrophenanthrene, DHP, quantum yields in fluid media.[6] Evidence for a shallow energy minimum at $^1c^*$ has been inferred from its long fluorescence lifetime (17.2 ns) observed from supersonic beams of *cis*-stilbene vapor seeded in inert gas expansions.[7]

Early studies of *cis*-stilbene luminescence in fluid solutions were hampered by *trans*-stilbene present as an impurity or formed during the process of recording the spectrum. Since the fluorescence quantum yield of *trans*-stilbene, $\phi_{fl}{}^t$, is nearly 500-fold the fluorescence quantum yield of *cis*-stilbene, $\phi_{fc}{}^c$, *cis*-stilbene fluorescence is easily overwhelmed by emission from the trans isomer. We have overcome these difficulties by employing *n*-hexane solutions of highly purified *cis*-stilbene. Luminescence from such solutions at 30.0 °C was resolved by use of principal-component–self-modeling analysis into nearly equal areas of $^1c^*$ ($A_{fc}{}^c$) and $^1t^*$ ($A_{fl}{}^c$) fluorescence, the latter stemming from adiabatic $^1c^* \rightarrow {}^1t^*$ conversion.[8] In our two preliminary reports, the adiabatic nature of $^1t^*$ formation was demonstrated by (a) the independence of $A_{fc}{}^c/A_{fl}{}^c$ on excitation light intensity[8a] and (b) fluorescence excitation spectra that faithfully track the *cis*-stilbene absorption spectrum, independent of monitored emission wavelength.[8b] Since adiabatic formation of $^1t^*$ was, to say the least, unexpected, it is important to stress that the fluorescence excitation spectra of *cis*-stilbene solutions obtained by monitoring the intensity at λ_{em} = 350 nm, the λ_{max} of $^1t^*$ fluorescence, were found to be composed primarily (~85%) of *cis*-stilbene excitation.[8b,c] The remaining (~15%) *trans*-stilbene excitation component was in quantitative agreement with the known 0.021% trans impurity.[8b,c] The details of the study of fluorescence excitation spectra[8c] will be presented in a separate paper. The present paper gives a full account of our emission results including the T effect on *cis*-stilbene-d_0 and -d_2 fluorescence quantum yields, $\phi_{fc}{}^c$ and $\phi_{fl}{}^c$, in *n*-hexane, C_6, and *n*-tetradecane, C_{14}. The observations allow the first experimental estimates of the $^1c^* \rightarrow {}^1p^*$ intrinsic barrier and the energy of $^1p^*$.

Experimental Section

Materials. *trans*-Stilbene-d_0 from Metron Laboratories, 99.99% purity, was used as received. *trans*-Stilbene-d_2 was synthesized from *cis*-stilbene-d_2 obtained by deuteration of diphenylacetylene, Aldrich, 99%, mp 59.0 °C, over Lindlar's catalyst using D_2, Matheson, 99.9% purity, at 1 atm pressure.[9] The solvent was methanol, Fisher, reagent grade, distilled and dried with 3 Å molecular sieves prior to use. Yields up to 95% were obtained using 3% catalyst (w/w) relative to diphenylacetylene. More catalyst increased the rate of reaction but promoted bibenzyl-d_4 formation. Following filtration through Celite and solvent evaporation, the mixture of *cis*-stilbene-d_2, bibenzyl-d_4, and unreacted diphenylacetylene was dissolved in toluene, Fisher, reagent grade, and the *cis*-stilbene-d_2 was isomerized to *trans*-stilbene-d_2 using a crystal of iodine, J.T. Baker, in refluxing toluene. Zinc powder, Matheson Coleman and Bell, was added with swirling until the characteristic purple color of iodine disappeared. The solution was filtered to remove the zinc iodide, and the reaction mixture was chromatographed on Wöelm acid alumina activity I, deactivated with 2% water (w/w).[10] Pentane, Fisher, reagent grade, was distilled and used as eluent to remove bibenzyl, followed by 20% distilled toluene in pentane (v/v) to elute the *trans*-stilbene-d_2. The *trans*-stilbene-d_2 was sublimed twice; purity by GLC analysis was 99.96%. *cis*-Stilbene-d_0 was synthesized from *trans*-stilbene, Aldrich, 96% purity. The *trans*-stilbene was first chromatographed, as described above, to remove bibenzyl prior to fluorenone-sensitized photoisomerization.[11] Fluorenone, Aldrich, was chromatographed on Fisher acid-washed alumina with benzene as eluent and recrystallized twice from methanol prior to use. The photostationary mixture of the stilbenes and fluorenone was chromatographed on Wöelm activity I acid or neutral alumina, deactivated with 2% water (w/w). Gravity feed of eluent, not flash chromatography, gave best separation. Repeated chromatography of the same sample was required to achieve 99.98% *cis*-stilbene purity. *cis*-Stilbene-d_2 was prepared from *trans*-stilbene-d_2, 99.96%, using the same procedure. Final purity of the *cis*-stilbene-d_2 was 99.99+% based on GLC analysis. All steps during the purification of *cis*-stilbene-d_0 and -d_2 were carried out in the dark or under red light. Glassware used was washed in a heated tank with Micro cleaner, rinsed three times with tap water, three times with distilled water, and twice with ethanol, and dried overnight in a low-temperature oven. It was rinsed with Fisher HPLC grade *n*-hexane immediately before use.

The solvents used for the emission studies were *n*-hexane, Fisher HPLC, and *n*-tetradecane, Aldrich 99+% purity. *n*-Hexane was used as received but *n*-tetradecane was passed through Wöelm neutral alumina, activity I, until no absorbance remained above 260 nm relative to air in a 1-cm quartz cuvette. All volumetric glassware including transfer pipets and volumetric flasks were analytical grade. Stilbene and 9,10-diphenylanthracene samples were weighed into volumetric flasks using a Mettler AE240 balance.

Analytical Procedure. GLC analyses were performed using a Varian 3300 capillary gas chromatograph equipped with a J&W Scientific Durowax DB-5 capillary column.[11] Programmed temperature range was 160.0 to 185.0 °C with a ramp rate of 1.0 °C/min. The carrier gas pressure was 16 psi. Typical retention times were: bibenzyl, 7.0 min; *cis*-stilbene, 7.2 min; diphenylacetylene, 15.4 min; and *trans*-stilbene, 18.6 min. Reduction of diphenylacetylene was followed by GLC and ^1H NMR. Aliquots were filtered through Celite prior to GLC analysis. Stilbene fractions from the chromatography column were concentrated by gentle heating on a hot plate under a stream of N_2 prior to injection. Final purity determination of *cis*-stilbene was made following bulb-to-bulb distillation under vacuum. GLC response was shown to be linear with stilbene concentration in the range employed by use of known *trans*-stilbene solutions containing biphenyl as internal standard.

Irradiation Procedure. A 450-W Hanovia medium-pressure mercury lamp, whose output was filtered through a uranyl glass filter, was used as the light source for the fluorenone-sensitized photoisomerization of *trans*-stilbene. Benzene, Mallinckrodt, spectral grade, was distilled and used as solvent initially. Later experiments employed *n*-hexane and benzene in a 14:1 (v/v) ratio. Fluorenone concentrations were 0.02 to 0.05 M in 390 mL of solvent. *trans*-Stilbene-d_0 and -d_2 were 5.7×10^{-2} M and 5.7×10^{-3} M, respectively. Product yields were limited by

(1) (a) Bagchi, B. *Int. Rev. Phys. Chem.* **1987**, *6*, 1. (b) Saltiel, J.; Sun, Y.-P. *Photochromism, Molecules and Systems*; Dürr, H., Bouas-Laurent, H., Eds.; Elsevier: Amsterdam, 1990; p 64 and references therein. (c) Bagchi, B.; Fleming, G. R. *J. Phys. Chem.* **1990**, *94*, 9. (d) Waldeck, D. H. *Chem. Rev.* **1991**, *91*, 415.

(2) (a) Saltiel, J. *J. Am. Chem. Soc.* **1967**, *89*, 1036; **1968**, *90*, 6394. (b) Orlandi, G.; Siebrand, W. *Chem. Phys. Lett.* **1975**, *30*, 352. (c) Hochstrasser, R. M. *Pure Appl. Chem.* **1980**, *52*, 2683.

(3) (a) Syage, J. A.; Lambert, W. R.; Felker, P. M.; Zewail, A. H.; Hochstrasser, R. M. *Chem. Phys. Lett.* **1982**, *88*, 266. (b) Syage, J. A.; Felker, P. M.; Zewail, A. H. *J. Chem. Phys.* **1984**, *81*, 4706. (c) Felker, P. M.; Zewail, A. H. *J. Phys. Chem.* **1985**, *89*, 5402.

(4) (a) Amirav, A.; Jortner, J. *Chem. Phys. Lett.* **1983**, *95*, 295. (b) Majors, T. J.; Even, U.; Jortner, J. *J. Chem. Phys.* **1984**, *81*, 2330. (c) Troe, J. *Chem. Phys. Lett.* **1985**, *114*, 241. (d) Schroeder, J.; Troe, J. *J. Phys. Chem.* **1986**, *90*, 4215.

(5) (a) Saltiel, J.; Sun, Y.-P. *J. Phys. Chem.* **1989**, *93*, 6246. (b) Sun, Y.-P.; Saltiel, J. *J. Phys. Chem.* **1989**, *93*, 8310. (c) Sun, Y.-P.; Saltiel, J.; Park, N. S.; Hoburg, E. A.; Waldeck, D. H. *J. Phys. Chem.* **1991**, *95*, 10,336.

(6) (a) Muszkat, K. A.; Gegiou, D.; Fischer, E. *J. Am. Chem. Soc.* **1967**, *89*, 4814. (b) Gegiou, D.; Muszkat, K. A.; Fischer, E. *J. Am. Chem. Soc.* **1968**, *90*, 12. (c) Wismontski-Knittel, T.; Fischer, G.; Fischer, E. *J. Chem. Soc., Perkin Trans. 2* **1974**, 1930.

(7) (a) Petek, H.; Fujiwara, Y.; Kim, D.; Yoshihara, K. *J. Am. Chem. Soc.* **1988**, *110*, 6269. (b) Petek, H.; Yoshihara, K.; Fujiwara, Y.; Frey, J. G. *J. Opt. Soc. Am. B* **1990**, *7*, 1540. (c) Petek, H.; Yoshihara, K.; Fujiwara, Y.; Lin, Z.; Penn, J.; Frederick, J. *J. Phys. Chem.* **1990**, *94*, 7539.

(8) (a) Saltiel, J.; Waller, A.; Sun, Y.-P.; Sears, D. F., Jr. *J. Am. Chem. Soc.* **1990**, *112*, 4580. (b) Saltiel, J.; Waller, A. S.; Sears, D. F., Jr. *J. Photochem. Photobiol. A: Chem.* **1992**, *65*, 29. (c) Waller, A. S. Ph.D. Dissertation, The Florida State University, 1992.

(9) Saltiel, J.; D'Agostino, J. T.; Herkstroeter, W. G.; Saint-Ruf, G.; Buu-Hoï, N. P. *J. Am. Chem. Soc.* **1973**, *95*, 2543.

(10) Perrin, D. D.; Armarego, W. L. F. *Purification of Laboratory Compounds*; Pergamon Press: New York, 1988; Vol. 3.

(11) Saltiel, J.; Ganapathy, S.; Werking, C. *J. Phys. Chem.* **1987**, *91*, 2755.

photostationary compositions, 85–89% cis, that were achieved within 1.5 h.

Absorption Spectra. UV absorption spectra were measured using a Perkin-Elmer Lambda-5 ultraviolet spectrophotometer with a scan rate of 60 nm/min, a slit of 2 nm, and a 0.2-s response. Spectra were measured at ambient temperature (~24 °C) using matched Hellma 1.00-cm Supracil quartz cells. Absorbance was recorded at 0.2-nm intervals on a Dell Corp. 12-MHz 80286/87 microcomputer.

Fluorescence Spectra. Luminescence measurements were made with a Hitachi/Perkin-Elmer MPF-2A spectrophotometer equipped with a 150-W Xe lamp and a Hamamatsu R-106UH photomultiplier tube, extensively modified to interface with a Dell Corp. 12-MHz 80286/87 microcomputer. Intensities were recorded at 1.0- or 2.0-nm increments for *cis*-stilbene emission spectra and 0.25 to 1.0 nm for the *trans*-stilbene and DPA emission spectra. Temperature control was provided by a Neslab RTE-4DD heating/cooling bath circulating water/ethylene glycol through a block surrounding the sample cell. For the flow cell the circulating fluid also passed through the outer jacket of the solution reservoir. Temperatures were constant to within ±0.2 °C as measured with an Omega Engineering Model 199 RTD digital thermometer.

Different cell mounts were used depending on the experiment. For flow cell experiments, a 1-cm quartz cell with inlet and outlet tubes sized for $^1/_4$-in. Teflon swagelok fittings was held firmly in a cell mount with a diagonally mounted set screw. A mirror opposite the PMT reflected stray emission light through the cell into the PMT. Temperature was monitored just above the excitation light path using an Omega platinum RTD probe placed in a Teflon swagelok fitting. The quartz flow cell was connected in series with Teflon tubing to a Teflon head pump and the flow cell reservoir. While data were taken, the solution was pumped through the cell at 10.3 to 14.7 mL s^{-1}. This procedure resulted in a controlled moderate rate of trans emission growth in the cis emission spectra. The flow reservoir was connected to the flow cell and then to the pump for measurements at higher temperatures in order to minimize the effect of bubbles formed when the solution passed through the pump head. Base-line emission spectra were recorded for the pure solvent at each λ_{exc} immediately before introduction of the stilbene solution into the reservoir and flow cell. The cell compartment was packed with foam insulation sealed with Saran Wrap and tape, and flushed with dry N_2 or Ar to minimize condensation on the cell walls for work below room temperature.

Static *trans*-stilbene and *cis*-stilbene emission spectra were obtained using a Hellma 1.00-cm Supracil quartz cell mounted in a modified Hitachi thermostated sample cell stage. Thermostated fluid from the Neslab circulator passed through a block in contact with two faces of the quartz cell. The thermometer probe was placed in a duplicate quartz cell housed in the same thermostated block. At least one emission spectrum was taken at 30.0 °C after every 10 spectra to monitor isomerization. No more than 20 spectra with any *n*-hexane solution and no more than 12 spectra with any *n*-tetradecane solution were measured. Excitation wavelength calibration was achieved by measuring the Rayleigh line for the 253.6-nm Hg line from a low-pressure pen lamp. This was essential for matching absorbances between standard and unknown solutions. *trans*-Stilbene, $\phi_{ft}^{t} = 0.0400 \pm 0.0011$ at 30.0 °C in C_6, was used as the fluorescence standard.[12] In order to optimize the weak *cis*-stilbene emission signal, larger than usual absorbances, 0.20–0.32 for 1.00-cm path length at λ_{exc}, were employed. In experiments where stilbene absorbances were not exactly matched at λ_{exc}, quantum yields obtained by adjusting for absorbance difference were in excellent agreement with quantum yields obtained using solutions with matched absorbance. Prior to base-line subtraction, scattered light from the pure solvent in the flow cell was corrected for variation in absorbance with λ that was caused when *cis*-stilbene was present as the solute. *trans*-Stilbene emission spectra were sufficiently intense that base-line subtraction was often superfluous. *cis*-Stilbene emission spectra from the static cell were measured using λ_{exc} = 338 and 345 nm. For these spectra the useful region was for $\lambda_{cm} \geq 360$ nm, and there was no need for base-line correction for transmittance of the *cis*-stilbene solutions. *cis*-Stilbene and *trans*-stilbene emission spectra were corrected for self-absorption at the blue edge of the emission by dividing observed emission intensity by solution transmittance assuming an effective path length of 0.5 cm (emission from the 1-cm cells was recorded at right angle to the excitation beam). Stilbene emission spectra were corrected for the transmission of the fluorimeter 290-nm cutoff filter that was employed. Correction factors for nonlinear instrumental response were obtained as described by Parker.[13] Details concerning all these procedures are given in ref 8c.

(12) Saltiel, J.; Waller, A. S.; Sears, D. F., Jr.; Garrett, C. Z. *J. Phys. Chem.*, in press.

(13) Parker, C. A. *Photoluminescence of Solutions*; Elsevier: Amsterdam, 1968; pp 252–258.

Table I. PCA–SM Spectral Matrices

cell	λ_{exc}, nm	λ_{cm} range,[a] nm	no. of spectra	expt
flow	268.0, 269.6, 272.0	310–596	76	1
flow	272.0	310–596	70	2
static	338.0	394–600	63	3

[a] Intensities were included at 2.0-nm increments.

Table II. Experimental Conditions for *cis*-Stilbene Emission Experiments[a]

expt, substrate, solvent	T, K	λ_{exc}, nm	λ_{cm} range, nm	[c] × 10^5, M	[t][b] × 10^5, M
1a, *c*-d_0, C_6	303.2	268.0–272.0	290–600	2.79	1.87
1b, *c*-d_2, C_6	303.2	268.0–272.0	290–600	2.78	1.73
2a, *c*-d_0, C_6	272.6–330.8	272.0	290–600	3.19	2.20
2b, *c*-d_2, C_6	272.6–330.8	272.0	290–600	2.84	1.72
3a, *c*-d_0, C_6	263.4–324.0	338.0	360–600	170	
3b, *c*-d_2, C_6	265.7–324.1	338.0	360–600	192	
4a, *c*-d_0, C_{14}	303.2–356.4	338.0	360–600	182	
4b, *c*-d_2, C_{14}	303.2–352.7	338.0	360–600	200	

[a] Experiments 1 and 2 in flow cell; expts 3 and 4 in static cell. [b] Standard *trans*-stilbene solution for quantum yield determination.

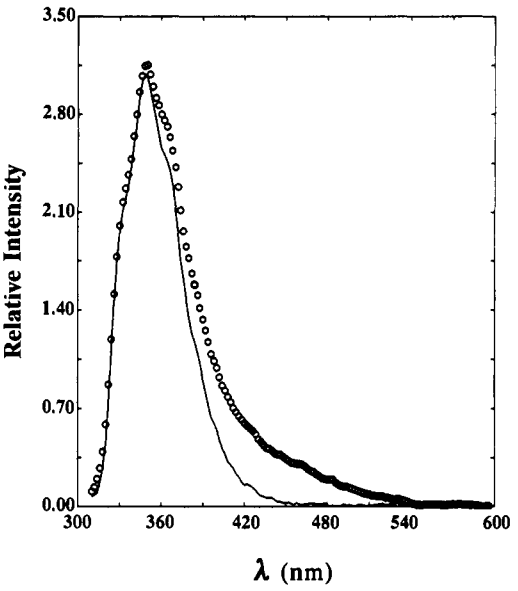

Figure 1. Average of 76 sequential emission spectra from a *cis*-stilbene-d_0 solution in C_6 at 30.0 °C (○), expt 1a, compared with *trans*-stilbene fluorescence (solid line) corrected at the blue edge for slight distortion due to absorption by a 2.79 × 10^{-5} M *cis*-stilbene solution.

Matrices for PCA–SM Calculations. Distortions due to Raman peaks were avoided by excluding the Raman peak region from the PCA–SM calculation. A description of spectral matrices employed in this study is given in Table I. More information concerning these experiments is given in the Results section.

Results

***cis*-Stilbene Fluorescence.** When excited in a region of significant *trans*-stilbene absorption, e.g., λ_{exc} = 270.0 nm, in static cells, the fluorescence spectrum from *cis*-stilbene solutions in C_6 appears identical with a *trans*-stilbene emission spectrum due to cis → trans photoisomerization. Interference due to *trans*-stilbene formation was minimized by use of a 4-mL quartz cell connected to a reservoir containing 500 mL of solution and a pump. The contribution of *trans*-stilbene fluorescence to the observed emission was dramatically reduced by continuous flushing of the excited solution out of the cell. In a typical experiment, the total spectral area prior to base-line subtraction increased only 15% during the course of recording 70 successive spectra (about 105-min irradiation in the spectrometer). Figure 1 shows the average of 76 spectra of 99.98% *cis*-stilbene in C_6 at 30.0 °C with λ_{exc} = 269.6 nm compared to a *trans*-stilbene spectrum with matched intensity

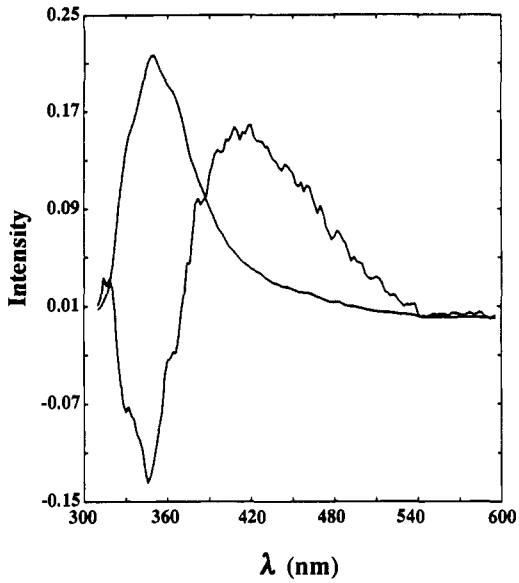

Figure 2. The two major eigenvectors from expt 1a; the relative magnitude of the four largest eigenvalues was $1.0:8.7 \times 10^{-3}:3.8 \times 10^{-4}:2.6 \times 10^{-4}$.

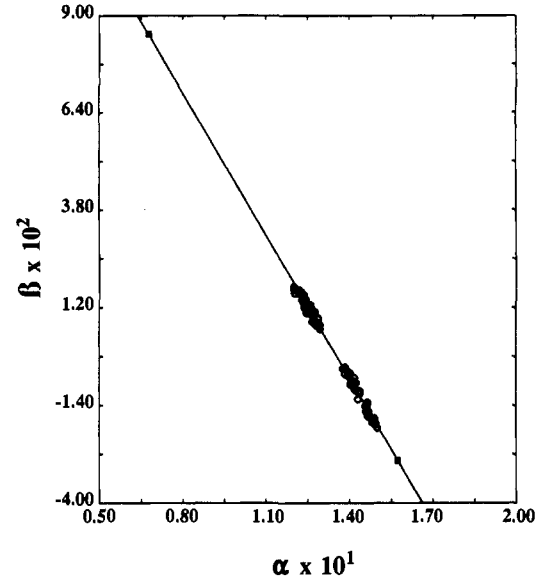

Figure 3. Normalization line of the vectors in Figure 2. The circles are combination coefficients for the spectra of the input matrix and the squares are pure component combination coefficients for *cis*- (upper) and *trans*-stilbene (lower).

at 310 nm. The spectra show a clear difference at $\lambda_{em} > 360$ nm. The *cis*-stilbene fluorescence spectrum was resolved by use of principal-component analysis with self-modeling (PCA–SM)[14] on matrices of spectra consisting of different contributions of *cis*- and *trans*-stilbene fluorescence. The experiments performed are described in Table II. The *trans*-stilbene concentrations listed in Table II were for solutions used as fluorescence standards. Fluorescence spectra were measured before and after each of three 1-mL portions of the *trans*-stilbene standard solution was added in the reservoir containing the *cis*-stilbene solution under study. In addition to this controlled increase in *trans*-stilbene concentration (up to 1.16×10^{-7} M in expt 1a), there was a slow increase due to cis → trans photoisomerization during the course of the measurements.

Matrices of baseline corrected, normalized emission spectra from these experiments were treated with PCA–SM and separated into *trans*-stilbene and *cis*-stilbene spectral emission components. Ratios of eigenvalues were indicative of two-component systems with the possible exception of expts 2a and 2b. In the latter case, the contribution of the third eigenvector may compensate for enhanced structure in the *trans*-stilbene fluorescence spectrum with decreasing T. Figure 2 shows the two major eigenvectors from expt 1a. They are nearly identical in appearance to those of expts 1b, 2a, and 2b. Combination coefficients (α_i, β_i) for the experimental spectra cluster tightly around the normalization line as shown in Figure 3.

The *trans*-stilbene spectral limit was obtained by subtracting the average of the first 10 spectra without added trans from the average of the last 10 spectra following the addition of the last *trans*-stilbene aliquot. Dot products of the resulting difference spectrum with the eigenvectors gave (α_t, β_t) combination coefficients that lie precisely on the normalization line. This difference spectrum is slightly distorted at its blue edge owing to "self-absorption" by the *cis*-stilbene solution. It was shown to be identical with the fluorescence spectrum of pure *trans*-stilbene when analytically corrected for this distortion.

The *cis*-stilbene emission spectrum could, in principle, be determined by using the criterion of zero spectral intensity at the onset region of the spectra, 310–340 nm.[14] In practice, residual emission at the 320-nm region that appeared to be part of the pure component *cis*-stilbene spectrum hampered the search for the cis limit. The intensity of the ~320-nm region decreased in size with repeated purification of *cis*-stilbene but could not be entirely eliminated. The minimum fractional contributions of the 320-nm peak were 5 and 8% of the pure component spectra of *cis*-stilbene-d_0 and -d_2, respectively. Attempts to treat the 320-nm peak as a third component failed, and it was artificially removed and replaced by a smooth curve at the onset of $^1c^*$ emission (see Figure 1, ref 8a). The resulting uncorrected $^1c^*$ spectrum, smoothed 10 times, is a structureless curve in the 337- to 550-nm region with $\lambda_{max} = 404$ nm. Spectra for *cis*-stilbene-d_0 and -d_2 are identical within experimental error (Figure 4).

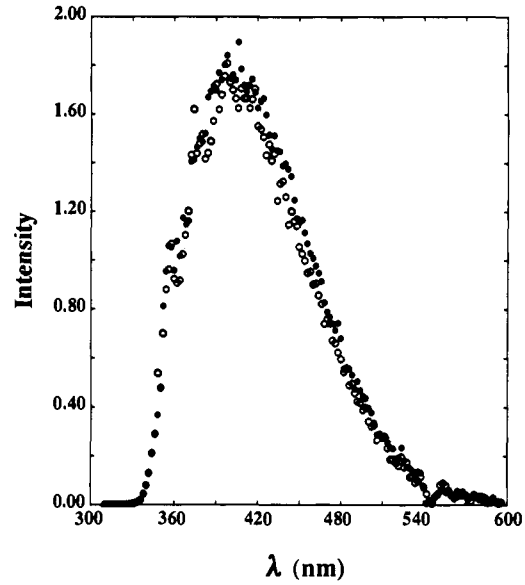

Figure 4. Pure component $^1c^*$ fluorescence spectra for *cis*-d_0 (●) and *cis*-d_2 (○) in C_6 at 30.0 °C; PCA–SM cis limits from expts 2a and 2b, respectively, uncorrected for nonlinearity in instrument response.

Once pure component coefficients were identified on the normalization lines, the experimental spectra were readily decomposed into cis and trans fractional contributions which when multiplied by the total area of each spectrum (normalization number) gave $^1c^*$ and $^1t^*$ fluorescence areas, A_c^c and A_t, respectively. After correction of A_t for increases due to the addition of successive trans aliquots, plots of A_t versus spectral number are roughly linear and reflect the slow increase in $^1t^*$ emission due to cis → trans isomerization. The data for expts 1a and 1b are plotted in Figure 5. The intercepts give the $^1t^*$ fluorescence areas prior to trans buildup.

(14) Sun, Y.-P.; Sears, D. F., Jr.; Saltiel, J. *Anal. Chem.* **1987**, *59*, 2515.

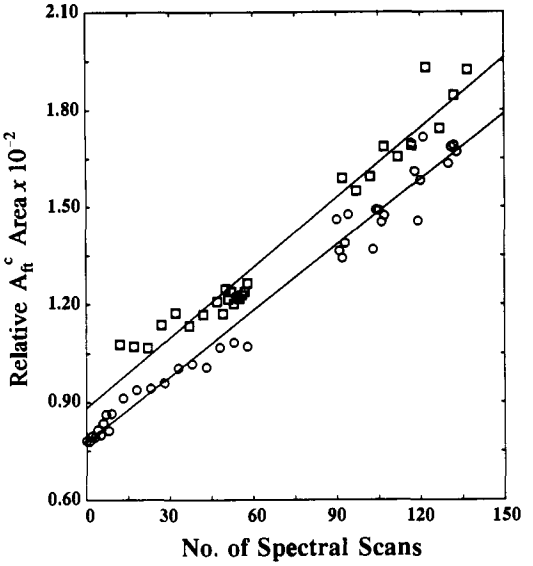

Figure 5. Increase in *trans*-stilbene spectral area, A_{ft}, as more spectra are taken for *cis*-stilbene-d_0 (○), expt 1a, and *cis*-stilbene-d_2 (□), expt 1b, in C_6 at 30.0 °C. Each spectral scan corresponds to 90-s irradiation in the spectrophotometer.

Selection of pure component combination coefficients for the cis fluorescence spectrum was refined by using the criterion of minimum change in A_c^c for each experiment at the selected T and λ_{exc}. Fluorescence areas, A_t^t, from standard *trans*-stilbene solutions with matched absorbance at λ_{exc} were used for quantum yield determinations. The criterion of minimum change in A_c^c gives slightly different trans limits for expts 2a and 2b at each temperature. This refinement was not necessary in experiments employing λ_{exc} = 338 nm since the portion of the fluorescence spectrum treated included only the structureless tails of $^1t^*$ emission starting at 394 nm. A series of 20 emission spectra was measured at each T starting with the pure *cis*-stilbene solution, and the *trans*-stilbene spectral limit was obtained by subtracting the initial spectrum from the final spectrum. This procedure resulted in uniform A_c^c values for each T.

Spectra from expts 4a and 4b were also corrected for a small buildup of phenanthrene fluorescence. Phenanthrene buildup was quantitatively determined following the taking of 20 spectra at 338 nm by measuring fluorescence spectra, 310–600 nm, of a diluted aliquot of the solution, 1:50, with λ_{exc} = 250 and 300 nm. The excitation wavelengths were selected so that the difference in ratios of molar absorptivities of *trans*-stilbene and phenanthrene was maximized. The 300-nm spectrum was nearly pure *trans*-stilbene fluorescence, containing no phenanthrene emission, whereas the 250-nm spectrum, where phenanthrene has its λ_{max} in the UV spectrum, contained a measurable contribution of phenanthrene emission. The 250-nm spectrum was separated into *trans*-stilbene and phenanthrene contributions by matching the 300-nm spectrum to its blue edge (310–340 nm) and subtracting. The resulting difference spectrum was identical with the spectrum of a standard phenanthrene solution. The phenanthrene:*trans*-stilbene fluorescence area ratio was used to calculate the concentration ratio of these products which was shown to remain constant during the course of measuring 1 to 20 spectra. The concentration ratio was then used to correct the 338-nm spectra for phenanthrene fluorescence. For instance, in expt 4a the fluorescence buildup observed in the λ_{exc} = 338 nm spectra in the 394–600-nm region consisted of 11.1% phenanthrene and 88.9% *trans*-stilbene fluorescence. A_t^c values prior to buildup were obtained by extrapolation as described above (see Figure 5); they required no correction for the presence of *trans*-stilbene impurity since initial *trans*-stilbene absorbance was negligible at 338 nm. Calculations were carried out on uncorrected spectra. However, final fluorescence areas were based on spectra corrected for nonlinearity of instrumental response and adjusted to include the entire spectral region from 310 to 360 nm. Significantly, A_t^c/A_c^c ratios obtained were, within experimental uncertainty, independent of λ_{exc} used for the experiments in Table II.

Table III. A_t Dependence on Added *trans*-Stilbene

experiment 1a			experiment 1b		
$[t\text{-}d_0]^a \times 10^4$, M	A_t^b	$(A_t/A_t^t)^c \times 10^2$	$[t\text{-}d_2] \times 10^4$, M	A_t^b	$(A_t/A_t^t)^c \times 10^2$
0.00	74.9(32)	0.212	0.00	88.7(69)	0.162
3.73	144.8(84)	0.410	3.45	185.8(40)	0.340
7.45	218.0(104)	0.618	6.89	292.0(88)	0.534
11.15	284.0(19)	0.805	10.32	398.9(123)	0.729

[a] Added *trans*-stilbene-d_0 and -d_2 concentrations; in expt 1a actual concentrations are 5.86×10^{-9} M higher, based on GLC analysis of *cis*-stilbene-d_0. [b] Values in parentheses are uncertainties in last significant figures shown. [c] Relative areas are based on $A_t^t = 3.53 \times 10^4$ and 5.47×10^4, the areas of the corrected fluorescence spectra of the standard *trans*-stilbene solutions for expts 1a and 1b, respectively.

Table IV. Neutral Density Filter Effect on *cis*-Stilbene Fluorescence Composition

filter absorbance	relative I_{exc}	% cis area[a]	% cis area[b] biphotonic trans
0.000	1.00	48.7	48.7
0.168	0.63	48.5	62.7
0.268	0.54	48.2	67.6
0.436	0.34	48.0	89.2

[a] Observed in C_6 at 30.0 °C. [b] Expected, if trans emission were biphotonic.

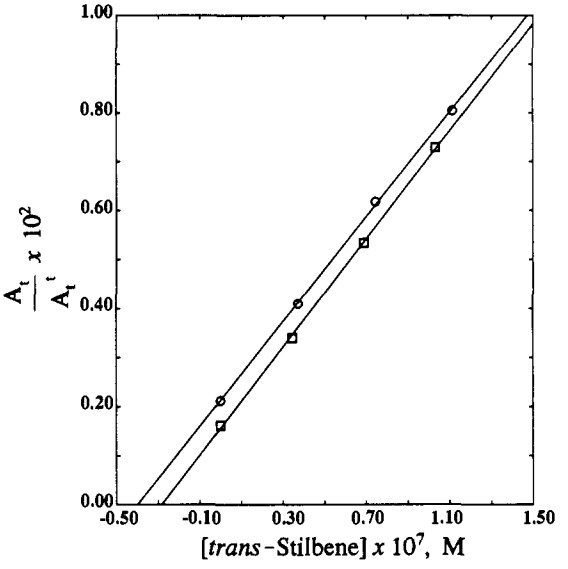

Figure 6. Increase in relative trans-fluorescence area, A_{ft}^{rel}, with added *trans*-stilbene concentration in the emission spectra of *cis*-stilbene-d_0 (○), expt 1a, and *cis*-stilbene-d_2 (□), expt 1b, in C_6 at 30.0 °C.

The A_t's from expts 1a and 1b, corrected for trans buildup using the slopes in the plots in Figure 5, are shown in Table III. They are plotted versus added *trans*-stilbene concentration in Figure 6. The intercept/slope ratios of these plots predict initial *trans*-stilbene concentrations of 3.99×10^{-8} and 2.84×10^{-8} M for expts 1a and 1b, respectively. These levels of *trans*-stilbene would correspond to 0.143 and 0.102% trans impurities in the *cis*-stilbene-d_0 and -d_2 samples, well in excess of the GLC determined levels of 0.021 and 0.00%, respectively.

As a further evaluation of the source of the excess trans emission in the *cis*-stilbene fluorescence spectra, the effect of attenuating exciting light intensity, I_{exc}, with neutral density filters was determined. The pure *cis*-stilbene solution from expt 1a was used and the percent contribution of the $^1c^*$ fluorescence determined (Table IV). The spectral shape is strictly independent of I_{exc}; see also Figure 7.

Fluorescence Quantum Yields. *cis*-Stilbene fluorescence quantum yields, ϕ_{fc}^c, were determined using *trans*-stilbene ϕ_{ft}^t = 0.0400 ± 0.0011 in C_6 at 30.0 °C as standard.[12] Corrections for

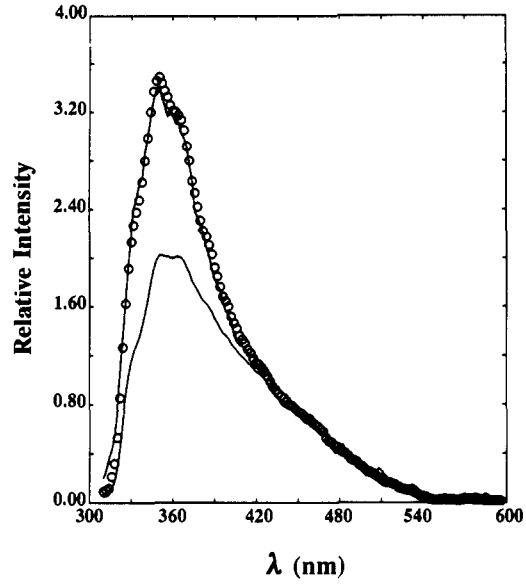

Figure 7. Average of 10 fluorescence spectra from a *cis*-stilbene-d_0 solution in C_6 at 30.0 °C measured with a neutral density filter (A = 0.268) in the excitation beam (O) compared with the spectra expected if the trans emission contribution is monophotonic (upper curve) or biphotonic (lower curve). The conditions are those of expt 1a; the three spectra were made to coincide in the 450–600-nm region where only $^1c^*$ emits.

differences in index of refraction, n, and absorbance, A, at λ_{exc} were applied as required using

$$\phi_{fc}^{c} = \phi_{ft}\frac{A_c}{A_t}\frac{A_t}{A_c}\frac{n_c^2}{n_t^2} \quad (1)$$

where the fluorescence areas A_t and A_c are corrected for nonlinearity in instrumental response.[13] The index of refraction and density of C_6 and C_{14} were calculated as previously described[12] using literature data.[15] The n^2 correction in eq 1 was applied in relating quantum yields in C_{14} to quantum yields in C_6. In addition, n^2 and density corrections were applied at different T's in the same solvent.[16]

Five independent determinations in C_6 at 30.0 °C and one at 30.2 °C with λ_{exc} in the 266.0–272.0-nm range gave satisfactorily reproducible ϕ_{fc}^{c} values in the (7.55 ± 0.36–8.76 ± 0.34) × 10^{-5} range. The average of these values, (8.13 ± 0.40) × 10^{-5} is slightly smaller than the value reported in our preliminary communication[8a] because of adjustment in the L_0/L ratio for DPA and to the refinement of the *trans*-stilbene limit in the PCA–SM analysis. The most complete experiments, expts 1 and 2, Table II, give ϕ_{fc}^{c} = (8.23 ± 0.31) × 10^{-5} and (8.04 ± 0.31) × 10^{-5} for *cis*-stilbene-d_0 and -d_2, respectively, in C_6 at 30.0 °C, relative to ϕ_{ft}^{t} = 0.0400, for *trans*-stilbene-d_0. After correction for 0.021% trans impurity in the *cis*-stilbene-d_0 sample, ϕ_{ft}^{c} = (7.3 ± 0.4) × 10^{-5} and (7.2 ± 0.2) × 10^{-5} were obtained from expts 1a and 2a, respectively, for *cis*-stilbene-d_0. Under the same conditions, ϕ_{ft}^{c} = (10.0 ± 0.7) × 10^{-5} was obtained from expt 1b for *cis*-stilbene-d_2. Determination of this quantity from expt 2b was not pursued because of the presence of a small unknown impurity emission in the region of *trans*-stilbene fluorescence. The ϕ_{fc}^{c} values in C_{14} at 30.0 °C were obtained relative to ϕ_{fc}^{c} = 8.13 × 10^{-5} for *c*-d_0 in C_6. Two sets of independent experiments gave ϕ_{fc}^{c} = (1.18 ± 0.07) × 10^{-4} and (1.27 ± 0.07) × 10^{-4} for *cis*-stilbene-d_0 and -d_2, respectively. Quantum yields of fluorescence for the *cis*-stilbenes in C_6 and C_{14} are shown as a function of T in Table V relative to ϕ_{fc}^{c} = 8.13 × 10^{-5} at 30.0 °C for both *c*-d_0 and *c*-d_2 in C_6.

Table V. Stilbene-d_0 and -d_2 Fluorescence Quantum Yields in *n*-Hexane and *n*-Tetradecane[a]

system	T, K	$\phi_{fc}^{c} \times 10^5$	$\phi_{ft}^{c} \times 10^5$	$\phi_{ft}^{t} \times 10^{2\,b}$	$\phi_{ct} \times 10^3$
C_6, d_0	330.8	7.9(2)	9.3(2)	2.2_7	4.1(1)
	324.3	7.2(4)	11.6(7)[c]	2.5_8	4.5(3)
	324.0	7.7(2)	8.6(11)	2.5_9	3.3(4)
	312.2	8.0(3)	8.0(7)	3.2_9	2.4(2)
	310.7	7.6(3)	12.7(12)[c]	3.6_7	3.4(3)
	303.4	8.1(3)	9.1(3)	3.9_8	2.3(1)
	303.2	8.13(40)	8.6(9)	4.0_0	2.2(2)
	302.9	8.1(1)	8.9(8)	4.0_2	2.2(2)
	293.9	8.1(3)	7.9(1)	4.9_2	1.6(2)
	284.8	8.0(2)	5.9(2)[c]	6.1_0	1.0(1)
	273.5	8.4(3)	8.7(15)	8.0_7	1.1(2)
	272.6	8.5(3)	9.2(2)	8.2_6	1.1(2)
	263.4	10.0(5)	8.9(15)	10.4_9	$0.8_5(1_5)$
		ave	8.7(3)		
C_{14}, d_0	356.4	7.2(6)	9.5(10)[c]	2.3_9	4.0(4)
	353.8	7.3(5)	13.1(12)	2.5_1	5.2(5)
	350.5	7.8(5)	7.9(10)[c]	2.6_8	3.0(4)
	347.9	7.8(3)	12.7(17)	2.8_2	4.5(6)
	344.0	8.1(4)	14.1(10)	3.0_5	4.6(3)
	342.5	8.1(5)	9.0(7)[c]	3.1_5	2.9(2)
	336.7	8.5(4)	13.5(12)	3.5_6	3.8(4)
	332.8	8.4(3)	14.0(13)	3.8_7	3.6(3)
	332.5	8.7(4)	13.6(20)	3.8_9	3.5(5)
	324.1	9.4(4)	13.9(17)	4.6_8	3.0(4)
	318.4	10.2(4)	13.1(20)	5.3_3	2.5(4)
	317.2	10.2(3)	14.8(3)	5.4_8	2.7(3)
	314.8	9.9(4)	12.5(6)	5.8_0	2.2(1)
	314.0	10.8(1)	17.6(6)[c]	5.9_1	3.0(1)
	308.3	11.3(3)	13.3(14)	6.7_7	2.0(3)
	308.1	11.7(7)	12.8(13)	6.8_0	1.9(2)
	303.2	11.8(5)	13.8(6)	7.6_6	1.8(1)
		ave	13.4(5)		
C_6, d_2	330.8	7.3(3)	9.7(4)	3.5_9	2.7(1)
	324.1	8.0(4)	11.2(8)	4.1_0	2.6(2)
	312.2	8.0(3)	10.6(4)	5.2_5	2.0(1)
	310.7	8.0(4)	18.5(13)[c]	5.4_2	3.4(3)
	303.2	8.1(4)	10.0(5)	6.3_9	1.6(1)
	294.7	8.7(3)[c]	11.3(14)	7.7_5	1.5(2)
	293.9	8.3(2)	10.0(6)	7.9_0	1.3(1)
	290.4	8.9(2)	11.3(13)	8.5_8	1.3(2)
	284.9	8.9(2)[c]	8.9(10)[c]	9.7_8	0.9(1)
	276.3	*d*	11.1(10)	12.0_8	0.9(1)
	274.2	8.9(3)	8.2(8)[c]	12.7_3	0.6(1)
	265.7	8.1(1)	1.7(8)[c]	15.8_1	0.1(1)
		ave	10.6(5)		
C_{14}, d_2	352.7	8.7(3)	17.4(11)[c]	3.65	4.8(3)
	346.4	8.6(4)	21.6(7)	4.4_0	4.9(2)
	336.3	9.2(3)	22.3(13)	5.1_9	4.3(3)
	327.8	9.5(5)	23.3(10)	6.2_9	3.7(2)
	317.2	11.1(4)	21.9(7)	8.0_7	2.7(1)
	312.8	11.0(3)	23.9(16)	8.9_8	2.7(2)
	308.3	11.9(5)	21.5(7)	10.0_3	2.1(1)
	303.2	12.8(6)	22.2(6)	11.3_9	2.0(1)
		ave	22.4(8)		

[a] *cis*-Stilbene-d_0 and -d_2 quantum yields relative to ϕ_{ft}^{t} = 0.0400 for *trans*-stilbene-d_0 in C_6 at 303.2 K; values in parentheses are estimated uncertainties in last significant digit(s) shown. [b] Interpolated values from treatment of ϕ_{ft}^{t} as a function of T.[12] [c] Not used in treatment of data due to difficulties in correcting for cis → trans photoisomerization. [d] Large 320-nm fluorescence contamination.

Discussion

The Source of *cis*-Stilbene Fluorescence. *cis*-Stilbene fluorescence spectra had been obtained previously from *cis*-stilbene in rigid organic glasses at low T[17–21] and from supersonic beams

(15) Timmermans, J. *Physico-Chemical Constants of Pure Organic Compounds*; Elsevier: New York, 1950; Vol. I.
(16) Saltiel, J.; Marinari, A.; Chang, D. W.-L.; Mitchener, J. C.; Megarity, E. D. *J. Am. Chem. Soc.* **1979**, *101*, 2982.

(17) (a) Stegemeyer, H.; Perkampus, H. H. *Z. Phys. Chem. (Munich)* **1963**, *39*, 125. (b) Aurich, F.; Hauser, M.; Lippert, E.; Stegemeyer, H. *Z. Phys. Chem. (Munich)* **1964**, *42*, 123. (c) Lippert, E. *Z. Phys. Chem. (Munich)* **1964**, *42*, 125.
(18) Lamola, A. A.; Hammond, G. S.; Mallory, F. B. *Photochem. Photobiol.* **1965**, *4*, 259.
(19) Sharafi, S.; Muszkat, K. A. *J. Am. Chem. Soc.* **1971**, *93*, 4119.
(20) Fischer, G.; Seger, G.; Muszkat, K. A.; Fischer, E. *J. Chem. Soc., Perkin Trans. 2* **1975**, 1569.

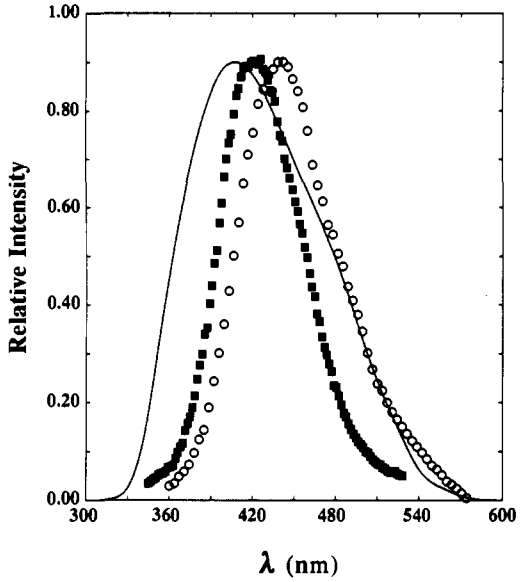

Figure 8. Comparison of $^1c^*$ fluorescence spectra from Figure 4, averaged, smoothed, and corrected for nonlinearity in instrumental response (—), with $^1c^*$ emission from a jet-cooled Ar cluster[7a] (■) and from a methylcyclohexane/3-methylpentane glass at 93 K (○).[20]

of *cis*-stilbene vapor seeded in inert gas expansions.[7] Assignment of these spectra to the $S_1 \rightarrow S_0$ transition of *cis*-stilbene is supported by their similarity to spectra of 1,2-diphenylcycloalkenes that serve as relatively rigid structural analogues of *cis*-stilbene.[18,21] We have used PCA–SM analysis to decompose the emission spectrum from a pure *cis*-stilbene solution in C_6 at 30.0 °C (Figure 7) into roughly equal areas of *trans*-stilbene fluorescence and a new featureless fluorescence spectrum (Figure 4) that is similar, but broader, than the earlier *cis*-stilbene fluorescence spectra (Figure 8). We assigned this spectrum to the $S_1 \rightarrow S_0$ transition of *cis*-stilbene in fluid solution and attribute its broader shape to emission from the greater range of cisoid geometries that are accessible to $^1c^*$ at the higher T and lower η employed in our study. Pulsed excitation transient absorption[22-24] and fluorescence studies[25] have established that the lifetime of $^1c^*$-d_0 in C_6 is 1.0 ps under our conditions. In view of this very short lifetime, some of the $^1c^*$ fluorescence may be occurring from vibrationally hot $^1c^*$ molecules and thus contributing intensity at the blue edge of the fluorescence spectrum. This conclusion has been based on theoretical calculations of the absorption and emission spectra of *cis*-stilbene.[25] It is necessary, therefore, to consider the possibility that the small 320-nm peak which we could not entirely eliminate from the pure component spectrum might represent a real feature of the *cis*-stilbene fluorescence spectrum. The varying contribution of this peak from experiment to experiment and the fact that its intensity was reduced by use of fresh C_6 or freshly distilled *cis*-stilbene are the strongest arguments for attributing this emission to an unknown impurity. Its spectral shape matches neither bibenzyl's nor phenanthrene's fluorescence spectrum,[26] and thus these two most likely contaminants of *cis*-stilbene can be discounted.

A precedent for fluorescence from vibrationally hot S_1 molecules is provided by benzophenone whose prompt fluorescence exhibits relatively stronger intensity at the higher energy bands of its diffuse vibrational progression than does its delayed fluorescence.[27] Presumably in this case the 10-ps lifetime of S_1 is too short to allow full vibrational relaxation prior to fluorescence from this state.[28]

The possibility that the blue edge of our 30.0 °C $^1c^*$ fluorescence spectrum in C_6 represents largely emission from vibrationally hot $^1c^*$ molecules[25] makes its use for the assignment of the $S_1 \leftarrow S_0$ origin less than straightforward. A long lifetime of 4.7 ns has been measured for $^1c^*$ fluorescence in 3-methylpentane glass at 77 K[29] under conditions that inhibit cis → trans photoisomerization and for which values of $\phi_{fc} = 0.75$–0.79 have been reported.[19,20] No doubt this emission originates from vibrationally relaxed $^1c^*$ molecules. The average of onset energies of emission and absorption spectra of *cis*-stilbene[21] give 82.9 ± 0.4 kcal/mol as 0^0 energy of the S_1–S_0 transition at 77 K in the rigid hydrocarbon glass. This is the value used by Todd et al. in the theoretical calculation of the spectra.[25] However, this origin is expected to shift to higher energy with increasing T owing, in part, to the decrease of the polarizability of the solvent. This phenomenon has been documented thoroughly for *trans*-stilbene and the vinylogous conjugated diphenylpolyenes.[30] For instance, in *trans*-stilbene the 0^0 band of the S_1–S_0 transition in a mixture of 2- and 3-methylpentanes shifts from 86.9 kcal/mol at 77 K to 87.8 kcal/mol at 295 K.[31] The range of reported values actually extends from 85.7 kcal/mol in bibenzyl crystal at 20 K[31] to 92.2 kcal/mol for jet-cooled isolated-molecule conditions.[3,4,32] In addition to these shifts in the origins of the S_0–S_1 transitions, the spectra of both stilbene isomers show pronounced red shifts of the λ_{max} and increases in transition probability with cooling that are attributed to a decrease in population of low-frequency modes involving torsional vibrations of the olefin–phenyl bonds.[19,33-38] A decrease in C–Ph torsion angles is also imposed by the rigidity of the glassy medium. The origin of the S_1–S_0 transition in the fluorescence spectrum of jet-cooled *cis*-stilbene in an Ar cluster has been estimated at ≤83.3 kcal/mol under conditions for which the well-resolved 0^0 band in *trans*-stilbene fluorescence is at 88.5 kcal/mol.[7] Thus our estimate of 85.7 kcal/mol for *cis*-stilbene in C_6 at 303.2 K based on the average of onset energies of absorption and fluorescence spectra may be somewhat high.

Adiabatic *trans*-Stilbene Fluorescence. *trans*-Stilbene fluorescence observed following excitation of *cis*-stilbene solutions is proportional to the concentration of $^1t^*$ at the moment the spectrum is recorded. Three possible sources of $^1t^*$ emission were considered: (1) excitation of *trans*-stilbene present as an impurity in the *cis*-stilbene sample, (2) excitation of *trans*-stilbene formed by photoisomerization of *cis*-stilbene in the course of recording the spectrum, and/or (3) formation of $^1t^*$ from $^1c^*$ via an excited-state pathway.

Quantitative analysis of *cis*-stilbene samples by GLC and by PCA–SM treatment of fluorescence excitation spectra[8b,c] are in exact agreement, showing the presence of (0.020 ± 0.001)% *trans*-stilbene in our *cis*-stilbene-d_0. Under the same conditions, no *trans*-stilbene was detected by GLC in *cis*-stilbene-d_2. It is only necessary to correct *cis*-stilbene-d_0 fluorescence spectra ob-

(21) Hohlneicher, G.; Müller, M.; Demmer, M.; Lex, J.; Penn, J. H.; Gan, L.; Loesel, P. D. *J. Am. Chem. Soc.* **1988**, *110*, 4483.
(22) Greene, B. I.; Scott, T. W. *Chem. Phys. Lett.* **1984**, *106*, 399.
(23) (a) Doany, F. E.; Hochstrasser, R. M.; Greene, B. I.; Millard, R. R. *Chem. Phys. Lett.* **1985**, *118*, 1. (b) Abrash, S.; Repinec, S.; Hochstrasser, R. M. *J. Chem. Phys.* **1990**, *93*, 1041.
(24) Todd, D. C.; Jean, J. M.; Rosenthal, S. J.; Ruggiero, A. J.; Yang, D.; Fleming, G. R. *J. Chem. Phys.* **1990**, *93*, 8658.
(25) Todd, D. C.; Fleming, G. R.; Jean, J. M. *J. Chem. Phys.* **1992**, *97*, 8915.
(26) Berlman, I. B. *Handbook of Fluorescence Spectra of Aromatic Molecules*, 2nd ed.; Academic Press: New York, 1971.
(27) Sun, Y.-P.; Sears, D. F., Jr.; Saltiel, J. *J. Am. Chem. Soc.* **1989**, *111*, 706.
(28) Greene, B. I.; Hochstrasser, R. M.; Weisman, R. B. *J. Chem. Phys.* **1979**, *70*, 1247.
(29) Yoshihara, K.; Namiki, A.; Sumitani, M.; Nakashima, N. *J. Chem. Phys.* **1979**, *71*, 2892.
(30) Sklar, L. A.; Hudson, B.; Petersen, M.; Diamond, J. *Biochemistry* **1977**, *16*, 813.
(31) Dyck, R. H.; McClure, D. S. *J. Chem. Phys.* **1962**, *36*, 2326.
(32) Champagne, B. B.; Pfanstiel, J. F.; Plusquellic, D. F.; Pratt, D. W.; van Herpen, W. M.; Meerts, W. L. *J. Phys. Chem.* **1990**, *94*, 6.
(33) Beal, R. N.; Roe, E. M. F. *J. Chem. Soc.* **1953**, 2775.
(34) Gegiou, D.; Muszkat, K. A.; Fischer, E. *J. Am. Chem. Soc.* **1968**, *90*, 3907.
(35) Saltiel, J.; D'Agostino, J. T. *J. Am. Chem. Soc.* **1972**, *94*, 6445.
(36) Bomberg, A.; Muszkat, K. A. *Tetrahedron* **1972**, *28*, 1265.
(37) Vogel, J.; Schneider, S.; Dörr, F.; Lemmen, P.; Lenoir, D. *Chem. Phys.* **1984**, *90*, 387.
(38) Ogawa, K.; Suzuki, H.; Futakami, M. *J. Chem. Soc., Perkin Trans. 2* **1988**, 39.

Table VI. *cis*-Stilbene Radiative Rate Constants[a]

conditions	ϕ_{fc}^c	τ_f, ps	$k_f \times 10^7$, s^{-1}	$(k_f/n^2) \times 10^7$, s^{-1}	$(k_f/n^{1.65}) \times 10^7$, s^{-1}
3-MP glass 77 K[b]	0.75–0.79	4.7×10^3	16.4	≤7.8	≤8.6
Ar cluster, gas[c]	≤1	17.2×10^3	≤5.8	≤5.8	≤5.8
C_6, 293 K[d]	8.3×10^{-5}	1.04	8.0	4.2	4.7
C_{14}, 293 K[d]	13.3×10^{-5}	1.52	8.7	4.3	4.8
C_{14}, *c*-d_2, 293 K[d]	14.1×10^{-5}	1.73	8.2	4.0	4.5

[a] Unless otherwise indicated, these are for *c*-d_0. [b] See refs 19 and 20 for ϕ_{fc}^c and ref 29 for τ_f; $n \geq 1.45$ was assumed. [c] Jet-cooled *c*-d_0.[7] [d] Fitted ϕ_{fc}^c using parameters in Table VII; τ_f from ref 24b and 25; see text.

tained with the shorter λ_{exc} for ~15% contribution to A_t by trans impurity in calculating ϕ_{ft}^c values. No such correction is required when $\lambda_{exc} \geq 338$ nm is employed owing to the negligible *trans*-stilbene absorbance at these wavelengths.

Excitation of *trans*-stilbene formed by photoisomerization of *cis*-stilbene in the light beam of the fluorimeter is the dominant source of fluorescence when *cis*-stilbene solutions are excited at $\lambda_{exc} \leq 330$ nm in a static cuvette. The purity of the cis isomer aside, this pathway could readily account for previous failures to detect the weak $^1c^*$ fluorescence in fluid solutions. The contribution of $^1t^*$ formation from this source was minimized by either the use of the flow cell or by employing $\lambda_{exc} \geq 338$ nm. For instance, in expts 1a and 1b, Table II, the increase in A_t with each spectrum taken under flow cell conditions is only 0.87 and 0.82%, respectively (Figure 5). In these experiments, the initial trans emission from the pure *cis*-stilbene solutions is linearly dependent on light intensity as is the cis emission (Table IV, Figure 7). This rules out the possibility that photoisomerization of *cis*-stilbene produces a significant *trans*-stilbene steady-state concentration in the illuminated region that is excited by a second photon to $^1t^*$. Clearly, under our extremely low photon fluxes such a process would lead to second-order dependence on I_{exc}. Also convincing of the adiabatic nature of $^1t^*$ emission is the fact that excitation of *cis*-stilbene solutions at $\lambda_{exc} = 345$ nm where *trans*-stilbene is transparent gives fluorescence spectra that are independent of the presence of purposely added or photochemically formed *trans*-stilbene. Though, admittedly, the useful spectral region is limited because of severe interference by scattered light, it overlaps the $^1t^*$ spectrum sufficiently to show that the A_t^c contribution at the red portion of the spectrum is independent of λ_{exc}. The useful spectral range is extended somewhat (394–600 nm) by using $\lambda_{exc} = 338$ nm. This allows use of a static cell to measure fluorescence quantum yields, but at the expense of observable trans buildup reflected in A_t. The increases in A_t per spectrum were 3.5, 4.1, 14.6, and 10.1% in expts 3a, 3b, 4a, and 4b, respectively. Again, the initial spectrum measured shows the identical $^1t^*$ fluorescence as impurity-corrected spectra obtained at shorter λ_{exc} (Figure 9). That the λ_{exc} independence of A_c^c and A_t^c is maintained over the entire *cis*-stilbene spectral absorption range was established via the PCA–SM resolution of fluorescence excitation spectra.[8b,c] A preliminary report of this work has appeared.[8b] Thus all our observations lead to the conclusion that a small but significant fraction of $^1c^*$ molecules reach $^1t^*$ via an excited-state pathway. As will be shown below, sources of this emission involving formation of $^1t^*$ from ground state ^1t are also inconsistent with the T independence of ϕ_{ft}^c values (Table V).

Radiative Rate Constants. Empirical radiative rate constants, k_f, can be based on eq 4 provided that fluorescence lifetimes, τ_f,

$$k_f = \Phi_f \tau_f^{-1} \tag{2}$$

and quantum yields are determined under the same conditions. For strongly allowed transitions a theoretical calculation of k_f can be based on the Strickler–Berg equation,[39]

$$k_f = 2.889 \times 10^{-9} n^2 \int_0^\infty f(\bar{\nu})\, d\bar{\nu} \left(\int_0^\infty f(\bar{\nu}) \bar{\nu}^{-3}\, d\bar{\nu} \right)^{-1} \int_0^\infty \frac{\epsilon(\bar{\nu})\, d\bar{\nu}}{\bar{\nu}} \tag{3}$$

where $f(\nu)$ and $\epsilon(\nu)$ are the fluorescence intensity and the molar absorptivity at frequency ν in cm^{-1}. Prior to this work, two estimates of the radiative rate constant for the $S_1 \rightarrow S_0$ transition of ^1c-d_0 were available. The first, $k_f = (1.64 \pm 0.05) \times 10^8$ s^{-1},

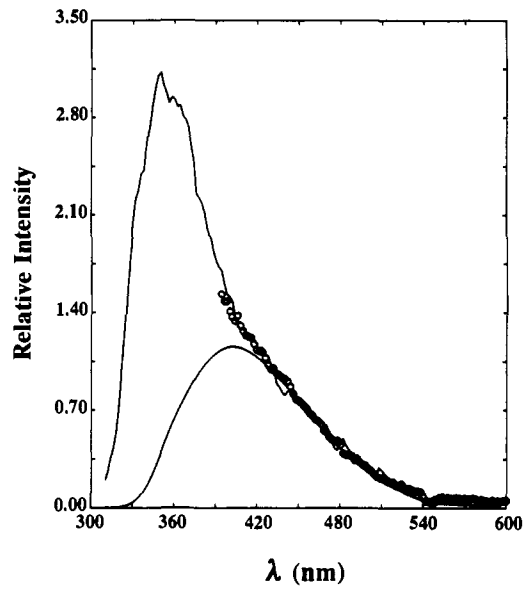

Figure 9. The emission spectrum of a pure *cis*-stilbene solution in C_6 (smooth curve) obtained with $\lambda_{exc} = 269.6$ nm, expt 1a (corrected for trans impurity and trans build up), compared with the spectrum obtained with $\lambda_{exc} = 338.0$ nm, expt 3a (O); the lowest curve is pure component $^1c^*$ fluorescence.

is based on the 4.7-ns lifetime of $^1c^*$ at 77 K in 3-methylpentane glass[29] and $\phi_{fc} = 0.75$–0.79 obtained under similar conditions.[19,20] The second, $k_f \leq 5.8 \times 10^7$ s^{-1}, is based on the 17.2-ns lifetime of $^1c^*$-d_0 fluorescence for *cis*-stilbene in an Ar cluster under jet-cooled conditions assuming $\phi_{fc} \leq 1.0$.[7] The most recent femtosecond-pulse excitation measurements of the lifetime of $^1c^*$ in C_6 are in excellent agreement, giving $\tau_f = 1.05 \pm 0.05$ ps (transient absorption decay at 650 nm) at ambient temperature[23b] and $\tau_f = 1.03 \pm 0.15$ ps (fluorescence up-conversion) at 293 ± 1 K.[24] Our interpolated $\phi_{fc}^c = 8.30 \times 10^{-5}$ for C_6 at 293 K (see below), together with the average $\tau_f = 1.04$ ps, gives $k_f = 8.0 \times 10^7$ s^{-1}. The difference in fluorescence lifetimes of $^1c^*$-d_0 of 1.38 ± 0.10 and 1.52 ± 0.05 ps obtained for $\lambda_{em} = 400$ nm and 430 nm, respectively, at 293 ± 1 K in C_{14} is probably not significant since the corresponding lifetimes for $^1c^*$-d_2, 1.72 ± 0.15 and 1.75 ± 0.10 ps show no λ_{em} dependence.[24] Though a lifetime of $^1c^*$-d_0 in C_{14} was not reported in the transient absorption studies,[23b] values obtained in C_{12} and in C_{16} are much more consistent with the 1.52-ps value. Using 1.52 ps and 1.73 ps as τ_f for $^1c^*$-d_0 and $^1c^*$-d_2, respectively, our extrapolated ϕ_{fc}^c values give $k_f = 8.7 \times 10^7$ s^{-1} and 8.2×10^7 s^{-1} in C_{14} at 293 K, in the same order.

A theoretical $k_f = 1.40 \times 10^8$ s^{-1} for both ^1c-d_0 and ^1c-d_2 in C_6 at 30.0 °C was obtained using the Strickler–Berg equation. The discrepancy between calculated and experimental k_f values is not surprising since the theoretical expression is not valid for molecules that have substantially different equilibrium geometries in S_1 and S_0 states.[39] Experimental k_f values are summarized in Table VI. Actually these different k_f's are in reasonably good agreement when differences in n are taken into account. Generally, the n dependence of the radiative rate constant can be expressed as

$$k_f = k_f^0 n^x \tag{4}$$

where k_f^0 is its value in the gas phase under isolated molecule

Table VII. Activation Parameters for $^1c^* \rightarrow {}^1p^*$ [a]

medium/stilbene	T range, K	E_{cp}[a], kcal/mol	$\Delta S_v/R + \ln(A_c/k_f^0\alpha_{cp})$	E_η, kcal/mol	$\ln A_\eta$
C_6, c-d_0, c-d_2	263.4–330.8	0.33(8)	27.80(13)	1.606(7)	−3.923(11)
C_{14}, c-d_0	303.2–356.4	1.90(8)	30.09(12)	3.277(20)	−4.801(30)
C_{14}, c-d_2[b]	303.2–346.4	1.86(15)	29.95(24)	3.277(20)	−4.801(30)
MCH/MCP, c-d_0	103.2–123.2	4.23(14)	39.83(63)[c]	5.97(24)	−17.906(1094)

[a] Values in parentheses are uncertainties in last significant digit(s) shown; viscosities in cP from ref 46 for C_6 and C_{14} and from refs 47 and 48 for MCH/MCP. [b] Treatment of k_{cp} excludes values for 312.8 and 352.7 K. [c] $k_{cp}\alpha_{cp} = 7.55 \times 10^7\ s^{-1}$ was used based on effective α_{cp} and k_f values of 0.87 and $8.7 \times 10^7\ s^{-1}$, respectively; see text.

Scheme I

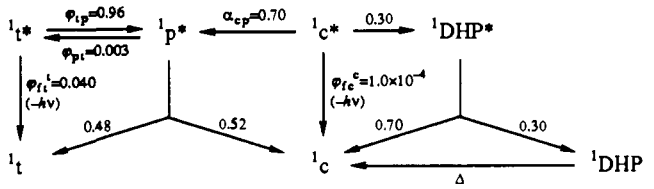

conditions for which $n = 1$, and x is expected to be close to 2 as predicted by the Strickler–Berg relationship.[39,40] A more complex theoretical expression for the n dependence of k_f, proposed by Shibuya,[41] predicts a somewhat lower effective x value, 1.7–1.8, for molecules such as meso-substituted anthracenes and *trans*-stilbene for which empirical tests of eq 6 are available.[12,40,42-45] Our recent analysis of ϕ_f and τ_f values for *trans*-stilbene in C_5, C_6, and C_{14} over a wide T range yielded $x = 1.65 \pm 0.08$.[12] Also shown in Table VI are k_f^0 values estimated assuming $x = 1.65$ and 2. The predicted radiative lifetimes under isolated molecule conditions 21.2 and 23.6 ns, respectively, are in reasonable agreement with the observed lifetime, 17.2 ns, for jet-cooled ^1c-d_2^* in Ar clusters. If $n = 1.0$ for the Ar clusters, exact agreement would be achieved for $x = 1.65$ and $x = 2$ if $\phi_{fc}^c = 0.81$ and 0.73, respectively, under those conditions.

Analysis of the *T* Dependence of ϕ_{fc}^c. It is well established that fluorescence from $^1c^*$ in fluid solution competes with two efficient radiationless reaction modes, one leading to *trans*-stilbene and the other to 4a,4b-dihydrophenanthrene, DHP. Extensive pho-

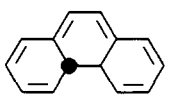

DHP

tochemical studies have been reviewed and are consistent with the fractional contributions of decay paths shown in Scheme I.[8b] The assumption in Scheme I that $^1p^*$ and ^{1}DHP* are true intermediates in the pathway to ^1t and DHP products has been questioned recently, since femtosecond-transient experiments suggest extremely rapid formation of ground-state products. For the purposes of this section, the detailed pathways to products are unimportant. The isomerization processes

$$^1c^* \xrightarrow{k_{cp}} {}^1p^* \tag{5}$$

$$^1c^* \xrightarrow{k_{cd}} {}^1\text{DHP}^* \tag{6}$$

can be understood as the radiationless, irreversible pathways that commit $^1c^*$ to ^1t and ^{1}DHP products, respectively. The analysis that follows relies on observations by Fischer and co-workers showing that in hydrocarbon solution the quantum yields of the two products are independent of T for $T \geq 253$ K.[6c] Since the work reported here was carried out at higher T's, it follows that the fraction of $^1c^*$ molecules that follow the relaxation pathway leading to ^1t is $\alpha_{cp} = k_{cp}/(k_{cp} + k_{cd}) = 0.70$, independent of T. It has been pointed out that when radiative decay competes with barrierless reactions, such as eq 5 and 6, the fluorescence quantum yield may not provide any direct information about the nonradiative decay rates.[1c] Use of the common definition of

$$\phi_{fc}^c = \frac{k_{fc}}{k_{fc} + k_{cp} + k_{cd}} \tag{7}$$

is justified in this case since ϕ_{fc}^c is independent of λ_{exc}, as is the decay rate of $^1c^*$ which is strictly monoexponential.[23,24] Accordingly, rate constants for the $^1c^* \rightarrow {}^1p^*$ process are given by

$$k_{cp} = k_{fc}\alpha_{cp}\left(\frac{\phi_{fc}^0 - \phi_{fc}^c}{\phi_{fc}^0\phi_{fc}^c}\right) \tag{8}$$

where $0.75 \leq \phi_{fc}^0 \leq 1$ is the limiting fluorescence quantum yield at very low T, and k_{fc} is given by eq 4 with $x = 1.7$.[6c,19,20] For the very small ϕ_{fc}^c's reported here, eq 8 reduces to

$$k_{cp} = k_{fc}\alpha_{cp}/\phi_{fc}^c \tag{9}$$

since the ϕ_{fc}^c's are negligible compared to ϕ_{fc}^0. Rate constants k_{cp} based on eq 9 with $k_f^0 = 4.7 \times 10^7\ s^{-1}$ and $x = 1.65$ in eq 4 are independent of deuterium substitution in C_6, but show a small deuterium effect in C_{14}. The rate constants for ^1c-d_0 and ^1c-d_2, treated together for C_6 and separately for C_{14}, were plotted according to the Arrhenius equation,

$$k_{cp} = A_{cp}e^{-E_{cp}^a/RT} \tag{10}$$

Figure 10, and give the activation parameters in Table VII.

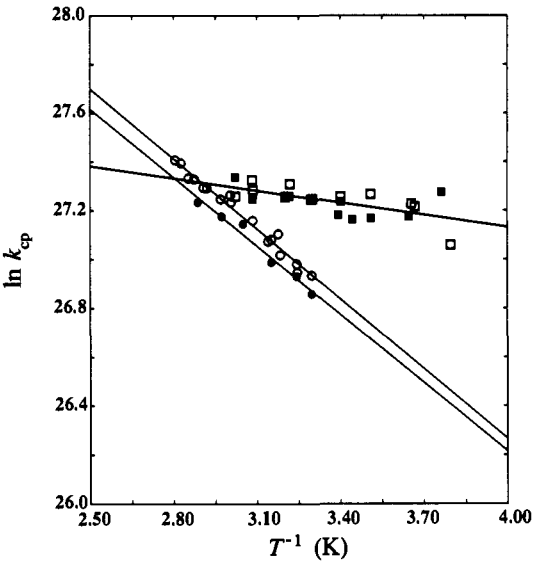

Figure 10. Arrhenius plots of k_{cp} in C_6, squares, and C_{14}, circles, for cis-d_0, open symbols, and cis-d_2, closed symbols.

(39) (a) Strickler, S. J.; Berg, R. A. *J. Chem. Phys.* **1962**, *37*, 814. (b) Birks, J. B.; Dyson, D. J. *Proc. R. Soc. London, Ser. A* **1963**, *275*, 135.
(40) Hirayama, S.; Phillips, D. *J. Photochem.* **1980**, *12*, 139.
(41) Shibuya, T. *Chem. Phys. Lett.* **1983**, *103*, 46.
(42) Lampert, R. A.; Meech, S. R.; Metcalfe, J.; Phillips, D.; Schaap, A. P. *Chem. Phys. Lett.* **1984**, *94*, 137.
(43) Maciejewski, A.; Steer, R. P. *J. Photochem.* **1986**, *35*, 59.
(44) Hirayama, S.; Iuchi, Y.; Tanaka, F.; Shobatake, K. *Chem. Phys.* **1990**, *144*, 401.
(45) Hirayama, S.; Yasuda, H.; Okamoto, M.; Tanaka, F. *J. Phys. Chem.* **1991**, *95*, 2971.
(46) American Petroleum Institute. *Selected Values of Physical and Thermodynamic Properties of Hydrocarbons and Related Compounds*; Carnegie Press: Pittsburgh, PA, 1953.

Since this work extends the observations of Fischer and colleagues[6c,19,20] from the high-viscosity to the low-viscosity regime, it was desirable to quantitatively relate their observations to our own. The fluorescence quantum yields of Sharafi and Muszkat in methylcyclohexane/methylcyclopentane, MCH/MCP (1:1), were selected for this purpose.[19] The treatment was confined to the 123.2–103.2 K region for which ϕ_{fc}^{c} increases monotonically from 0.012 to 0.25,[19] and for which experimental shear viscosities, η_s, are available[47,48] and adhere reasonably well to the Andrade equation,[49]

$$\eta_s = A_{\eta_s} e^{E_{\eta_s}/RT} \tag{11}$$

where E_{η_s} is the activation energy for viscous flow. Since the exact value of ϕ_{fc}^{0} is unknown, avoiding the lower T region has the advantage of making the treatment insensitive to the ϕ_{fc}^{0} value selected. One complication remains because in the selected T region both product quantum yields are T dependent and α_{cp} must vary.[6c] In the hydrocarbon mixture methylcyclohexane/2-methylpentane (2:1) for which nearly identical ϕ_{fc}^{c} values have been reported as in MCH/MCP near the glass transition in the T region of interest, the cis → trans quantum yield, ϕ_{ct}, drops from 0.30 to 0.17, while the corresponding drop in the cis → DHP quantum yield, ϕ_{cd}, is from 0.03 to 0.012.[6c] Based on Scheme I, we estimate that the corresponding change in α_{cp} is from 0.85 to 0.89. Since, furthermore, the index of refraction change is less than 1%,[50] it seems prudent to assume that both k_{fc} and α_{cp} are essentially constant. The plot of ln $[(\phi_{fc}^{0} - \phi_{fc}^{c})/\phi_{fc}^{0}\phi_{fc}^{c}]$ versus T^{-1} is linear and gives activation parameters that are included in Table VII.

The Medium Effect on k_{cp}. An excellent review of theoretical treatments of medium and T effects on barrierless reactions is available.[1c] An important theoretical prediction is a crossover from an apparent negative T dependence of the rate constant at small viscosity to positive activation energy at higher viscosity.[1c] Experimental verification of this prediction has been claimed most notably in studies of the radiationless decay rate constants of electronically excited triphenylmethane dyes, such as crystal violet, CV, in the *n*-alcohol solvent series.[52,53] In seeking the intrinsic

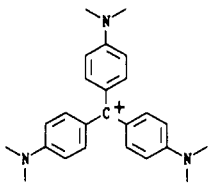

CV

activation energy of the torsional relaxation process, the usual practice has been to use a homologous solvent series and vary the temperature in order to determine decay rate constants at constant shear viscosity. The activation energy is then obtained from the slope of isoviscosity Arrhenius plots.[51,52] The identical procedure has also been employed for cases, such as the trans → cis photoisomerization of stilbene, that are subject to a positive intrinsic barrier.[1,5c] Such plots are based on the assumption that the friction coefficient, ξ_r, experienced by the twisting portion of the molecule is proportional to η_s of the medium in accord with the Stokes–Einstein hydrodynamic equation.[5c] The use of shear viscosity in this approximation has been shown to be a major source of failures of the Kramers' equation[53] in accounting for the medium and temperature dependencies of the rate constants for barrier crossing in the $^1t^* \rightarrow {}^1p^*$ direction.[5c] Much better agreement between experiment and theory is achieved when an effective viscosity[54] or a microviscosity, η_μ, based on a molecular probe[5b,55–57] of the viscosity are employed instead of η_s.[5c] A corollary to these findings is that the search for intrinsic activation energies should be based on isomicroviscosity rather than on isoviscosity Arrhenius or transition-state plots.[1b,5b,c]

An alternative approach to accounting for medium and T effects on radiationless decay processes that involve a significant change in solute geometry is the *medium-enhanced barrier model*.[1b,5a,35] This model has been applied successfully to the $^1t^* \rightarrow {}^1p^*$ decay process in *trans*-stilbene[5a,35] and should in principle be applicable to barrierless processes such as $^1c^* \rightarrow {}^1p^*$.[58] According to this model the overall torsional relaxation process can be represented by

$$(^1c^*S) \underset{}{\overset{K_s}{\rightleftharpoons}} (^1c^*S') \xrightarrow{k_c} (^1p^*S') \tag{12}$$

where S designates solvent cages that restrict rotation and S′ designates solvent cages that do not restrict rotation. The two solvent cage populations are assumed to interconvert rapidly compared to k_c and are related by equilibrium constant K_s. The effective decay rate constant is given by $k_{cp} = K_s k_c/(1 + K_s)$ which reduces to $k_{cp} = K_s k_c$ for $K_s \ll 1$. The analogous reduced form was applied for the $^1t^* \rightarrow {}^1p^*$ process, and, though the relaxation time scales are different, this limit will tentatively be applied to $^1c^* \rightarrow {}^1p^*$. Since the $^1c^* \rightarrow {}^1p^*$ process is close to the low-frequency reaction mode limit for which transition-state theory predicts Arrhenius-type behavior, k_c is given by

$$k_c = A_c e^{-E_c^{0}/RT} \tag{13}$$

where E_c^{0} is close to the intrinsic barrier. It follows that

$$k_{cp} = A_c e^{\Delta S_v/R} e^{-(E_c^{0} + \Delta H_v)/RT} \tag{14}$$

where ΔH_v and ΔS_v are the enthalpy and entropy changes associated with solvent cage interconversion. Comparison of eqs 10 and 14 shows that $E_{cp}^{a} = E_c^{0} + \Delta H_v$ and $A_{cp} = A_c e^{\Delta S_v/R}$. In cases where the viscosity obeys the Andrade equation, the relationship of ΔH_v to E_{η_s} can be obtained by combining eqs 11 and 14

$$\ln k_{cp} = \ln k_c + \frac{\Delta S_v}{R} + a \ln A_{\eta_s} - a \ln \eta_s \tag{15}$$

where $a = \Delta H_v/E_{\eta_s}$. At constant T eq 15 has the form of the frequently discussed power law equation (the first equal sign)

$$k_{cp} = \frac{k_c B}{\eta_s^{a}} = \frac{k_c f^{a} B}{\eta_\mu^{a}} \tag{16}$$

where B is a constant and $0 \le a \le 1$. Equation 16 was initially proposed as a semiempirical expression based on the free volume theory[6b,19] and was recently reintroduced as an empirical modification of the Smoluchowski limit ($a = 1$) of the Kramers' equation.[59] In the medium-enhanced barrier model a represents the fraction of the viscous flow activation energy that is experienced by the solute as an additional barrier. Actually, the use

(47) Greenspan, H.; Fischer, E. *J. Phys. Chem.* **1965**, *69*, 2466.
(48) von Salis, G. A.; Labhart, H. *J. Phys. Chem.* **1968**, *72*, 752.
(49) Use of the Andrade equation over a wider T region would be inappropriate since the extended Andrade plot shows pronounced curvature (ref 48).
(50) Charlton, J. L.; Saltiel, J. *J. Phys. Chem.* **1977**, *81*, 1940.
(51) (a) Sundström, V.; Gillbro, T.; Bergstrom, H. *Chem. Phys.* **1982**, *73*, 419. (b) Sundström, V.; Gillbro, T. *J. Chem. Phys.* **1984**, *81*, 3463.
(52) (a) Ben-Amotz, D.; Harris, C. B. *J. Chem. Phys.* **1987**, *86*, 4856, 5433. (b) Ben-Amotz, D.; Jeanloz, R.; Harris, C. B. *J. Chem. Phys.* **1987**, *86*, 6119.
(53) (a) Kramers, H. A. *Physica* **1940**, *7*, 284. (b) Chandrasekhar, S. *Rev. Mod. Phys.* **1943**, *15*, 1.
(54) (a) Lee, J.; Zhu, S.-B.; Robinson, G. W. *J. Phys. Chem.* **1987**, *91*, 4273. (b) Zhu, S.-B.; Lee, J.; Robinson, G. W. *J. Chem. Phys.* **1988**, *88*, 7088. (c) Robinson, G. W.; Singh, S.; Krishnan, R.; Zhu, S.-B.; Lee, J. *J. Phys. Chem.* **1990**, *94*, 4. (d) Zhu, S.-B.; Lee, J.; Robinson, G. W. *J. Phys. Chem.* **1991**, *95*, 1865.
(55) (a) McCaskill, J.; Gilbert, R. G. *Chem. Phys.* **1979**, *44*, 389. (b) Velsko, S. P.; Waldeck, D. H.; Fleming, G. R. *J. Chem. Phys.* **1983**, *78*, 249. (c) Zeglinski, D. M.; Waldeck, D. H. *J. Phys. Chem.* **1988**, *92*, 692.
(56) Lee, M.; Bain, A. J.; McCarthy, P. J.; Han, C. H.; Haseltine, J. N.; Smith, A. B.; Hochstrasser, R. M. *J. Chem. Phys.* **1986**, *85*, 4341.
(57) Bowman, R. M.; Eisenthal, K. B.; Millar, D. P. *J. Chem. Phys.* **1988**, *89*, 762.
(58) Dellinger, B.; Kasha, M. *Chem. Phys. Lett.* **1975**, *36*, 410; **1976**, *38*, 9.
(59) Velsko, S. P.; Fleming, G. R. *J. Chem. Phys.* **1982**, *76*, 3553.

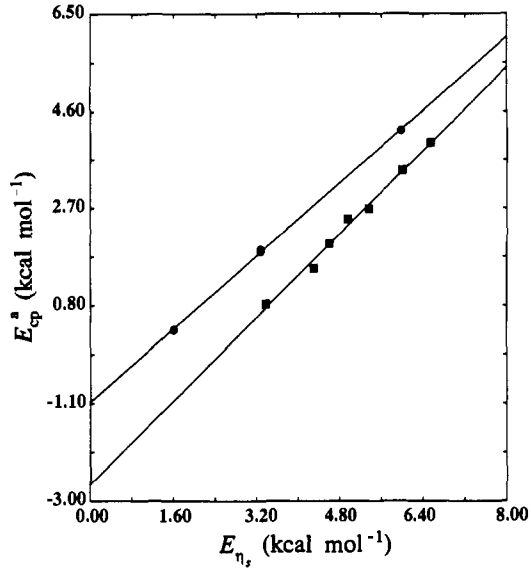

Figure 11. The dependence of $E_{cp}{}^{a}$ on E_{η} (●) and the corresponding plot for crystal violet (■) based on activation parameters in ref 53a.

of η_s in eq 16 does not give a directly, but a function of a and T.[5c] In fact, the usual practice of equating $-a$ to the slope of a ln k versus ln η_s plots at constant T underestimates a.[5c,60] Multiplication of both numerator and denominator by f^a, where f is the microfriction factor that converts η_s to η_μ, gives the analogous microviscosity expression shown after the second equal sign in eq 16, and a can be obtained from the slope of the ln k versus η_μ plot provided certain well-defined conditions apply.[5c] For instance, in the case of *trans*-stilbene in the *n*-alkane solvent series the identical a value is obtained from the plot of ΔH_{tp}^{*} versus E_{η_s} as from the plot of ln k_{tp} versus ln η_μ at constant T.[5b,61] Furthermore, the enhanced barrier model gives the same ΔH_t^{*} for the intrinsic barrier[5a] as do isomicroviscosity transition-state plots.[5b,61] The reason why the activation energy for viscous flow can be based on η_s instead of the more desirable η_μ is that the microfriction factor f is only weakly T dependent and corrects mainly the preexponential factor in the Andrade equation.[5c]

A plot of $E_{cp}{}^{a}$ versus E_{η_s} adheres to

$$E_{cp}{}^{a} = E_c{}^{0} + aE_{\eta_s} \qquad (17)$$

giving $E_c{}^{0} = -1.07 \pm 0.05$ kcal/mol and $a = 0.89 \pm 0.01$ (Figure 11). The negative intrinsic barrier corresponds to a hypothetical hydrocarbon medium for which $E_{\eta_s} = 0$, consistent with the absence of a barrier, and it is reasonable that, as the only resistance to torsional displacement in ^{1}c* comes from the medium, its radiationless decay experiences the activation energy for viscous flow fully, i.e., $a \simeq 1$. Although these conclusions could be derived from the low-viscosity C_6 and C_{14} data alone, it is gratifying that the high-viscosity data of Sharafi and Muszkat[19] are in agreement with our observations and that the treatment now extends over the wide viscosity range of 0.2 to 10^5 cP.

Negative activation energies for barrierless processes are consistent with theory[1c,62] and, as indicated above, have been found experimentally in torsional relaxation decay processes of dyes.[51,52,63] For instance, Arrhenius isoviscosity plots for CV in the *n*-alcohol series, C_1–C_8, in the 0.6- to 8-cP range have yielded apparent activation energies that are nearly independent of the viscosity employed ranging from −1.73 to −2.51 kcal/mol.[51] However, when the *n*-alcohol series is extended to longer alkyl group chains, C_{10}–C_{18}, the isoviscosity Arrhenius plots turn upward, suggesting a turnover to a positive activation energy.[51,53] Since rotational diffusion rate constants of molecules in long-chain alcohols show similar behavior,[64,65] we suspect that, to the extent that the friction coefficient of the solvent is the controlling factor, the turnover to a positive slope would be eliminated if isomicroviscosity plots were employed. In fact, an alternative microviscosity approach to our own,[5c] based on the theory of Gierer and Wirtz,[66] has been claimed to succeed in accounting for the medium effect on the torsional relaxation of triphenylmethane dyes.[67] However, the conclusions of this work are, to say the least, difficult to evaluate. At the very high medium-viscosity regions employed, biexponential decays were observed and the treatment was based on weighted lifetime averages whose physical significance is dubious. Furthermore, effective E_η values were used in medium regions where the Andrade plots show significant deviation from linearity (compare 1-propanol's $E_{\eta_s} = 6.5$ kcal/mol from ref 70 with $E_{\eta_s} = 4.3$ kcal/mol from ref 52a).

With the exception of methanol, the activation energies obtained for CV in the C_2–C_{10} *n*-alcohols[52] are in accord with eq 17 (Figure 11), and give an intrinsic activation energy $E_{cv}{}^{0} = -2.68 \pm 0.22$ kcal/mol and $a = 1.02 \pm 0.04$. It is especially significant that the activation energy in 1-decanol shows no deviation from eq 17, though individual decay rate constants in that solvent consistently deviate from isoviscosity plots.[51,52] The full imposition of the activation energy for viscous flow to the torsional relaxation process in CV is consistent with our observations on ^{1}c* and suggests that this may apply generally to barrierless torsional relaxation processes. The deviation of the methanol point from the enhanced-barrier model line in Figure 11 is not surprising since similar deviations have also been observed for ^{1}t* → ^{1}p* in *trans*-stilbene in methanol and ethanol.[1b]

There has been much discussion in the literature concerning the detailed nature of the ^{1}c* to ground-state trans reaction coordinate. The possibility that the process may be multidimensional is generally proposed to account for a rapidly increasing array of spectroscopic evidence.[7,23-25,68,69] These complex reaction coordinates include the suggestion that the initial ^{1}c* motions leading to trans isomer are along the reaction coordinate for photocyclization to DHP.[7c] It has also been speculated that out-of-plane C–H vibrations of the ethylenic moiety may play so significant a role, that the process may not be impeded strongly by solvent molecules.[23b] In fact, ^{1}c* decay times in different solvents have been interpreted to show a *weak* medium-viscosity dependence![24,25] Whatever the complexities of the actual reaction coordinate, application of the enhanced barrier model to the observations shows it to be fully coupled to the medium. This would be more easily understood if motions of the phenyl groups play a significant role along the reaction coordinate. It should be noted that the notion that the ^{1}c* → ^{1}DHP pathway should be less sensitive to medium friction than the ^{1}c* → ^{1}t pathway,[7c] though intuitively pleasing, is not borne out by quantum yield measurements in hydrocarbon glasses.[6c] The medium inhibits ^{1}c* → ^{1}DHP well before it affects ^{1}c* → ^{1}t.[6c]

Deuterium Isotope Effect on k_{cp}. An unusually large secondary deuterium isotope effect has been observed on the trans → cis isomerization of the highly strained *trans*-1-phenylcyclohexene upon substitution of its vinyl-H.[70] This is, in part, due to an

(60) The power law equation has also been used to relate observed rate constants at different T's in a single solvent to η_s. Comparison of eqs 15 and 16 shows that, since k_c varies with T, a more meaningful approach would be to plot ln (k_{cp}/k_c) instead of ln k_{cp} versus ln η_s (ref 8c).

(61) A more recent derivation of activation parameters for C_5, C_6, and C_{14} suggests that a for ^{1}t* → ^{1}p* may have to be revised upward from 0.39 to 0.41 and ΔH_t^{*} downward from 2.85 to 2.79 kcal/mol (ref 12).

(62) Bagchi, B.; Fleming, G. R.; Oxtoby, D. W. *J. Chem. Phys.* **1983**, *78*, 7375.

(63) For other discussions of negative activation energies, see: (a) Houk, K. N.; Rondan, N. G.; Mareda, J. *J. Am. Chem. Soc.* **1984**, *106*, 4291. (b) Houk, K. N.; Rondan, N. G. *J. Am. Chem. Soc.* **1984**, *106*, 4293. (c) Moss, R. A.; Lawrynowicz, W.; Turro, N. J.; Gould, I. R.; Cha, Y. *J. Am. Chem. Soc.* **1986**, *108*, 7028.

(64) Chuang, T. J.; Eisenthal, K. B. *Chem. Phys. Lett.* **1971**, *11*, 368.

(65) (a) Courtney, S. H.; Kim, S. K.; Canonica, S.; Fleming, G. R. *J. Chem. Soc., Faraday Trans. 2* **1986**, *82*, 2065. (b) Kim, S. K.; Fleming, G. R. *J. Phys. Chem.* **1988**, *92*, 2168.

(66) Gierer, A.; Wirtz, K. *Z. Naturforsch. A* **1953**, *8*, 532.

(67) Vogel, M.; Rettig, W. *Ber. Bunsenges. Phys. Chem.* **1987**, *91*, 1241.

(68) Myers, A. B.; Mathies, R. A. *J. Chem. Phys.* **1984**, *81*, 1552.

(69) (a) Sension, R. J.; Repinec, S. T.; Hochstrasser, R. M. *J. Phys. Chem.* **1991**, *95*, 2946. (b) Sension, R. J.; Repinec, S. T.; Hochstrasser, R. M. *J. Chem. Phys.* **1990**, *93*, 9185. (c) Repinec, S. T.; Sension, R. J.; Szarka, A. Z.; Hochstrasser, R. M. *J. Phys. Chem.* **1991**, *95*, 10,380.

increase in the activation energy for this reaction from 12.1 ± 0.12 kcal/mol to 12.8 ± 0.15 kcal/mol, k_H/k_D = 2.0 at room temperature.[70] It was proposed that the effect should be considered as quasi-primary since it probably reflects significant involvement of the out-of-plane C_e–H bend along the isomerization reaction coordinate.[70] It was predicted that large isotope effects should be found for other alkenes as well.[70] Indeed, a large effect, (k_{tpd_0}/k_{tpd_2}) = 1.5–1.6 at room temperature, has been found on the $^1t^* \rightarrow {}^1p^*$ process in *trans*-stilbene which is subject to a much smaller effective activation energy.[1b,8a,12,71] A study of the T dependence of τ_f for t-d_0 and t-d_2 revealed no change in the activation energy for $^1t^* \rightarrow {}^1p^*$ in several solvents, including C_6.[71] However, when the T dependence of fluorescence quantum yields is also considered and the n dependence of k_f is included in the treatment, the results suggest a slight increase in activation energy in C_6 and a somewhat larger increase in C_{14}, ΔE_{tp}^a = 0.32 kcal/mol, upon deuteration of the olefinic positions.[12] It was of interest therefore to examine the analogous d-effect on the $^1c^* \rightarrow {}^1p^*$ process. While this work was in progress, a small but significant effect on the lifetime of $^1c^*$ in C_{14} was observed upon deuteration of the olefinic hydrogens, $(\tau_{fd_2}/\tau_{fd_0})$ = 1.15 ± 0.10 at 20 °C.[24] It was suggested that this effect was an indication of intimate involvement of C_e–H vibrations along the reaction coordinate. Our results give $(\phi_{fcd_2}{}^c/\phi_{fcd_0}{}^c)$ = 1.08 ± 0.10 in C_{14} at 20 °C, which is, within experimental uncertainty, in very good agreement with the lifetime ratio. However, we discern no measurable d-effect on k_{cp} in C_6 where the effective reaction barrier is less than RT (Table VII). This suggests that the magnitude of the d-effect in olefin geometric isomerizations increases with increasing barrier height. The absence of a d-effect for $^1c^* \rightarrow {}^1p^*$ in C_6 is certainly sensible since no tunneling or changes in zero-point energies should contribute when a process is essentially barrierless.

The Energy of $^1p^*$. The data in Table V give $\phi_{ft}{}^c$ values for ^1c-d_0 and ^1c-d_2 in C_6 and in C_{14} that are remarkably T independent. In contrast, $\phi_{ft}{}^t$, over the T ranges employed, changes by factors of 3–4 (Table V). The differences in the T dependence of $\phi_{ft}{}^c$ and $\phi_{ft}{}^t$ provides additional evidence against the involvement of ground-state *trans*-stilbene as the source of the fluorescence of $^1t^*$ in pure ^1c solutions. Since $\phi_{ft}{}^c = \phi_{ct}\phi_{ft}{}^t$, the T dependencies of the efficiencies of adiabatic $^1t^*$ formation, ϕ_{ct}, must complement the T dependencies of $\phi_{ft}{}^t$ nearly exactly (Table V). As $\phi_{ft}{}^c$ and $\phi_{ft}{}^t$ are independent of λ_{exc}, ϕ_{ct} must likewise be λ_{exc} independent, and $^1c^* \rightarrow {}^1t^*$ does not measurably depend on the excess energy content of nascent $^1c^*$. This indicates very rapid vibrational relaxation of nascent $^1c^*$, and it may be relevant here that the relaxation channel of triphenylmethane dyes which, as pointed out above is barrierless, has also been found to be unusually efficient in transferring energy to the solvent bath.[52a]

The simplest pathway from $^1c^*$ to $^1t^*$ is along the potential energy surface for rotation about the central bond through the phantom singlet intermediate $^1p^*$. This mechanism gives $\phi_{ct} = \alpha_{cp}\phi_{pt}$, where $\phi_{pt} = k_{pt}\tau_p$ and α_{cp} = 0.70; see Scheme I. Assuming that the lifetime of $^1p^*$, τ_p, is T independent as has been demonstrated for the phantom triplet state, $^3p^*$,[72] the T dependence of k_{pt}, the rate constant for $^1p^* \rightarrow {}^1t^*$, is identical with the T dependence of ϕ_{ct}. Furthermore, since under our conditions most $^1t^*$ return to $^1p^*$, $^1t^*$ and $^1p^*$ can be considered to be in quasi-equilibrium. It follows that $^1t^*$ and $^1p^*$ represent essentially isoenergetic regions on the S_1 surfaces of stilbene-d_0 and -d_2 in C_6 and in C_{14}. Of course, more complex mechanisms can be imagined. For instance, the adiabatic $^1c^* \rightarrow {}^1t^*$ process may occur via a higher energy twisted electronic state, $^1p^{**}$, whose rapid decay to $^1p^*$ competes with $^1p^{**} \rightarrow {}^1t^*$. However, in the absence of experimental evidence supporting other pathways, we prefer the simplest mechanism.

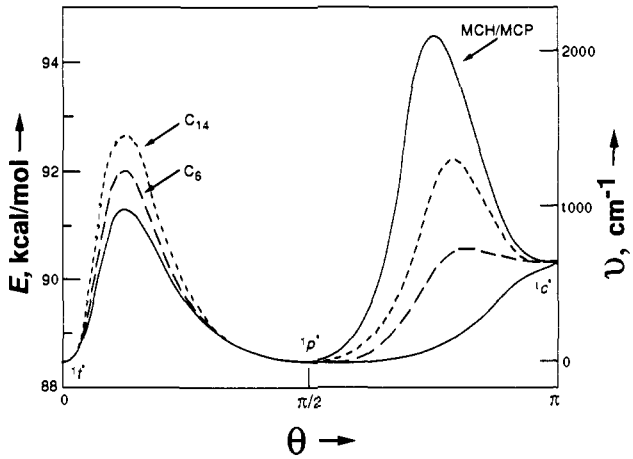

Figure 12. Schematic potential energy curves for the cis ⇄ trans reaction coordinate in different media.

The Shape of the Potential Energy Surface. Schematic potential energy curves for the cis ⇄ trans reaction coordinate in S_1 were constructed using the energies of $^1t^*$, $^1p^*$, and $^1c^*$ and the effective activation energies for torsional relaxation as anchor points (Figure 12). The energy difference between $^1t^*$ and $^1c^*$ is based in part on the corresponding ground-state energy difference for which the 4.6 ± 0.1 kcal/mol value in aromatic media was employed.[11] The energies of the $^1c^*$ side of Figure 12 would be 1.1 kcal/mol higher if the ground-state enthalpy difference for the liquid trans ⇄ liquid cis equilibrium were employed instead.[73] Although we have followed the usual practice of giving the energy as a function of the torsional angle θ about the central bond, exclusion of significant changes along other vibrational modes is not intended. The solid line in Figure 12 depicts the intrinsic energy surface in a hypothetical hydrocarbon solvent whose microfriction coefficient is zero, E_{η_s} = 0. We resisted the temptation to place $^1c^*$ in a shallow inherent energy minimum as has been suggested to account for the long-lived $^1c^*$ fluorescence from jet-cooled ^1c-d_0 in inert gas clusters[7] because we suspect that the barrier under these conditions is induced by the inert gas.[74] The dashed lines show effective potential energy curves in the different hydrocarbon media. These curves are consistent with the kinetics manifestations of the medium-enhanced barrier model which has received support in the theory of Dellinger and Kasha.[58] The calculation for a assumes that the same $E_c{}^0$ applies to each hydrocarbon medium. Application of the Hammond postulate to the $^1c^* \rightarrow {}^1p^*$ process suggests that the transition-state geometry should progressively move to larger torsional angles with increasing effective energy barrier.[75] If we adopt this view and let a = 1.00, then, $E_c{}^0 = E_{tp}{}^a - E_{\eta_s}$ is predicted to take the values −1.3, −1.4, and −1.7 kcal/mol in C_6, C_{14}, and MCH/MCP, respectively. This is shown schematically in Figure 12.

The Lifetime of $^1p^*$. An elegant demonstration of the involvement of $^1p^*$ as an intermediate that provides a significant bottleneck in trans → cis photoisomerization has been described for the rigid stilbene analogue, *trans*-1,1′-biindanylidene, *t*-B.[76]

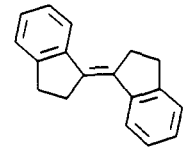

t-B

The key observation which led to assignment of a short-lived transient absorption at 351 nm to $^1p^*$-B is the increase in the amplitude of this absorption that accompanies the decrease in

(70) Caldwell, R. A.; Misawa, H.; Healy, E. F.; Dewar, M. J. S. *J. Am. Chem. Soc.* **1987**, *109*, 6869.
(71) Courtney, S. H.; Balk, M. W.; Philips, L. A.; Webb, S. P.; Yang, D.; Levy, D. H.; Fleming, G. R. *J. Chem. Phys.* **1988**, *89*, 6697.
(72) Görner, H.; Schulte-Frohlinde, D. *J. Phys. Chem.* **1981**, *85*, 1835.
(73) Williams, R. B. *J. Am. Chem. Soc.* **1942**, *64*, 1395.
(74) Brus, L. E.; Bondybey, V. E. *Chem. Phys. Lett.* **1975**, *36*, 252.
(75) Hammond, G. S. *J. Am. Chem. Soc.* **1955**, *77*, 334.
(76) Doany, F. E.; Heilweil, E. J.; Moore, R.; Hochstrasser, R. M. *J. Chem. Phys.* **1984**, *80*, 201.

medium viscosity.[76] Higher $^1p^*$ absorbance is observed in the lower viscosity solvents, C_6–C_{16} alkanes, at constant T, and at higher T in the same solvent consistent with the changes of feeding rates of $^1p^*$ from $^1t^*$. Kinetics analysis of the evolution of the 351-nm absorption was consistent with a medium-independent lifetime of $^1p^*$-B, $\tau_p = 10 \pm 3$ ps.[76]

In the parent stilbene molecule, an early estimate of $\tau_p = 3 \pm 2$ ps was based on the time evolution of transient absorption at 312.5 nm following excitation of ^1c-d_0.[23a] This was revised downward recently to $\tau_p \leq 0.15$ ps.[23b] Based on our simple mechanism, a rough estimate of τ_p can be obtained by setting $k_{tp} = k_{pt}$. This neglects any possible entropy difference between $^1t^*$ and $^1p^*$ and, based on the ϕ_{ct} data in Table V, the activation parameters in ref 12 for k_{tp}, and $\tau_p = \phi_{ct}/\alpha_{cp}k_{pt}$, gives $\tau_p = 0.26$ and 0.31 ps for $^1p^*$-d_0 in C_6 and in C_{14}, respectively, at 30 °C. The entry for $\phi_{ft}{}^c$ of ^1c-d_0 in C_6 given in Table V is about 20% larger than the values obtained from flow-cell experiments 1a and 2a. Use of these more reliable values gives $\tau_p = 0.21$ ps at 30 °C. If we assume that the deuterium isotope effect in the $^1p^* \rightarrow {}^1t^*$ direction is identical with that in the $^1t^* \rightarrow {}^1p^*$ direction, the same procedure gives $\tau_p = 0.40$ and 0.50 ps for ^1c-d_2 in C_6 and in C_{14}, respectively. This suggests that it should be easier to detect a bottleneck at $^1p^*$ in transient decay kinetics of $^1c^*$-d_2. An olefinic-position specific deuterium isotope effect was established previously for the decay of the twisted stilbene triplet, $^3p^*$.[2a,9,77]

The lifetimes inferred for $^1p^*$ are very close to the lifetime assigned by Greene et al. to isolated $^1c^*$ in the gas phase, $\tau = 0.32$ ps.[78] Since the $^1c^* \rightarrow {}^1p^*$ process should be barrierless under these conditions, the rate-determining step for the observed transient decay may be the radiationless decay of $^1p^*$ to the ground-state surface.

Acknowledgment. This research was supported by NSF Grant CHE 90-14060.

Registry Number supplied by author: **1a**, 17329-15-6.

(77) (a) Caldwell, R. A.; Cao, C. V. *J. Am. Chem. Soc.* **1982**, *104*, 6174. (b) Caldwell, R. A. *Pure Appl. Chem.* **1984**, *56*, 1967.
(78) Greene, B. I.; Farrow, R. C. *J. Chem. Phys.* **1983**, *78*, 3336.

Tautomeric Equilibrium and Hydrogen Shifts of Tetrazole in the Gas Phase and in Solution

Ming Wah Wong,* Regis Leung-Toung, and Curt Wentrup*

Contribution from the Chemistry Department, The University of Queensland, Brisbane, Queensland 4072, Australia. *Received October 5, 1992*

Abstract: High-level ab initio molecular orbital calculations, using basis sets up to 6-311+G(2d,2p) with electron correlation incorporated at the quadratic configuration interaction [QCISD(T)] level, have been used to study the tautomeric equilibrium and hydrogen shifts of tetrazole in the gas phase and in solution. The solvent effects were investigated by self-consistent reaction field (SCRF) theory. Consistent with experimental observations, the 1*H*-tetrazole (**1**)/2*H*-tetrazole (**2**) tautomeric equilibrium is calculated to be strongly influenced by the surrounding medium. 2*H*-Tetrazole is the energetically preferred tautomer in the gas phase. In a nonpolar solution, both the 1*H* and 2*H* forms are predicted to exist in comparable amounts. However, in a medium of high dielectric constant the more polar 1*H* tautomer is the dominant species. The calculated free energy changes for tautomerization of 1*H*-tetrazole in the gas phase and in nonpolar ($\epsilon = 2$) and polar ($\epsilon = 40$) media are −7, 1, and 12 kJ mol^{-1}, respectively. The molecular geometry, charge distribution, and vibrational frequencies of the polar 1*H* tautomer are found to be altered significantly in the presence of a solvent reaction field. Isomerization of **1** to **2**, via a [1,2] hydrogen shift, requires an energy barrier of 207 kJ mol^{-1} in the gas phase. 5*H*-Tetrazole (**3**) is predicted to lie 82 kJ mol^{-1} above **1**, due to its nonaromatic character. However, rearrangement of **3** to **1**, via a [1,5] hydrogen shift, is inhibited by an activation barrier of 150 kJ mol^{-1}. Conversely, the energy barrier for the rearrangement of **1** to **3** is 232 kJ mol^{-1}, slightly larger than that required for the isomerization of **1** to **2**. These results suggest that **3** is a good candidate for experimental observation. Inclusion of electron correlation leads to a drastic change in the molecular geometry of **3**. At the MP2 level, an acyclic structure is predicted, while at the MP3 and QCISD levels the expected cyclic structure is found. The calculated molecular geometry of 1*H*-tetrazole at the MP2 level is found to differ significantly from the available solid-state structural data.

Introduction

There has been considerable and continuing interest in the chemistry of tetrazoles.[1] In principle, three protomers of unsubstituted tetrazole are possible, namely 1*H*- (**1**), 2*H*- (**2**), and 5*H*-tetrazole (**3**) (Figure 1). Both **1** and **2** have been observed experimentally.[2-6] Results from X-ray crystallography unambiguously showed that tetrazole exists as the 1*H* tautomer (**1**) in the solid state.[2] In solution, there is an equilibrium between **1**

(1) (a) Benson, F. R. In *Heterocyclic Compounds*; Elderfield, R. C., Ed.; Wiley: New York, 1967; Vol. 8. (b) Grimmett, M. R. *Comprehensive Organic Chemistry*; Pergamon Press: New York, 1979; Vol. 4. (c) Butler, R. N. In *Comprehensive Heterocyclic Chemistry*; Katritzky, A. R., Rees, C. W., Eds.; Pergamon Press: New York, 1984; Vol. 5.

(2) van der Putten, N.; Heijdenrijk, D.; Schenk, H. *Cryst. Struct. Commun.* **1974**, 321.
(3) (a) Wofford, D. S.; Forkey, D. M.; Russell, J. G. *J. Org. Chem.* **1982**, *47*, 5132. (b) Charton, M. *J. Chem. Soc. B* **1969**, 1240. (c) Witanowski, M.; Stefaniak, L.; Januszewski, H.; Grabowski, Z.; Webb, G. A. *Tetrahedron* **1972**, *28*, 637. (d) Moore, D. G. W.; Whittaker, A. G. *J. Am. Chem. Soc.* **1960**, *82*, 5007. (e) Kaufman, M. H.; Ernsberger, F. M.; Ewans, W. S. *J. Am. Chem. Soc.* **1956**, *78*, 4197. (f) Henry, R. A. *J. Am. Chem. Soc.* **1951**, *73*, 4470. (g) Jensen, K. A.; Fredgier, A. K. *Dan. Vidensk. Selsk., Mat.*-Fys. *Medd.* **1943**, *20*, 1.
(4) Krugh, W. D.; Gold, L. P. *J. Mol. Spectrosc.* **1974**, *49*, 423.

0002-7863/93/1515-2465$04.00/0